AGU PUBLICATIONS

JGR

Journal of Geophysical Research: Oceans

RESEARCH ARTICLE

10.1002/2014JC010013

Key Points:
- Shelf water west of Spitsbergen is modified by Atlantic Water exchange
- Atlantic water melts drift ice on the shelf
- Buoyancy forcing rather than Ekman forcing drives cross-frontal overturning

Correspondence to:
V. Tverberg,
Vigdis.Tverberg@uin.no

Citation:
Tverberg, V., O. A. Nøst, C. Lydersen, and K. M. Kovacs (2014), Winter sea ice melting in the Atlantic Water subduction area, Svalbard Norway, *J. Geophys. Res. Oceans*, *119*, doi:10.1002/2014JC010013.

Received 3 APR 2014
Accepted 18 AUG 2014
Accepted article online 21 AUG 2014

Winter sea ice melting in the Atlantic Water subduction area, Svalbard Norway

V. Tverberg[1], O. A. Nøst[2], C. Lydersen[2], and K. M. Kovacs[2]

[1]Faculty of Biosciences and Aquaculture, University of Nordland, Bodø, Norway, [2]Norwegian Polar Institute, Fram Centre, Tromsø, Norway

Abstract Herein, we study a small area along the shelf west of Spitsbergen, near Prins Karls Forland, where warm, saline Atlantic Water of the West Spitsbergen Current currently first encounters sea ice. This sea ice is drifting in a coastal current that carries Arctic Water originating from the Barents Sea northward over the shelf. Our aim was to investigate whether melting of sea ice by Atlantic Water in this area might be a significant factor that could contribute to the formation of a cold halocline layer that isolates the sea ice from further melting from below. Observations of temperature and salinity profiles were collected during two winters, via CTD-SRDL instruments deployed on harbor seals (*Phoca vitulina*), and fed into a heat and freshwater budget box model in order to quantify the importance of melting relative to other processes that could transform the shelf water mass during winter. Cross-frontal exchange of Atlantic Water from the West Spitsbergen Current, driven by buoyancy forcing rather than Ekman upwelling, was determined to be the source of the heat that melted drift ice on the shelf. Some local sea ice formation did take place, but its importance in the total heat and freshwater budgets appeared to be minor. The data suggest that the production of a cold halocline layer was preceded by southerly winds and rapid drift ice melting.

1. Introduction

There is increasing recognition in the scientific community that the recent decline in Arctic sea ice might be linked to Atlantic Water inflow [*Ivanov et al*., 2012; *Alexev et al*., 2013]. Atlantic Water is a relatively warm, high-salinity water mass originating from the Gulf Stream. Atlantic Water enters the Arctic Ocean as branches from the Norwegian Atlantic Current, either through the Barents Sea or via the West Spitsbergen Current along the continental shelf slope west of Spitsbergen, with typical winter temperatures of 3–4°C, and salinity 35.1. At varying geographical location along the West Spitsbergen Current, Atlantic Water subducts below the Arctic sea ice cover while still retaining a large proportion of its heat, but a cold halocline layer protects the sea ice from being melted by the heat in the Atlantic Water layer.

Sea ice formation is believed to be the process that is most influential in the formation of the cold halocline layer. Varying degrees of salt rejection during ice formation explain the salinity stratification observed in this layer, while temperature is homogeneously cold throughout the layer [*Rudels et al*., 1996]. A typical salinity range for the cold halocline layer in the Arctic Ocean is 32.0–34.3 [*Rudels et al*., 1996], while in the Barents Sea it is more saline, forming the so-called Arctic Water that has a salinity range of 34.3–34.7 [*Loeng*, 1991]. Temperatures are close to freezing during winter, but increase during summer heating. *Steele et al*. [1995] suggests that sea ice melting in the Marginal Ice Zone during winter could also contribute to the formation of the cold halocline layer, but acknowledge that such melting is of negligible importance for the total volume that is formed. However, it might be possible that melting occurring directly in the subduction region where Atlantic Water meets sea ice could be important. Understanding the possible interplay between subduction of Atlantic Water and the formation of the cold halocline layer may therefore be crucial for making projections regarding sea ice conditions in a warming climate.

The west coast of Spitsbergen is an ideal region for studying melting of sea ice by Atlantic Water. The continental shelf west of Spitsbergen is a region that normally contains substantial amounts of drifting sea ice that follow the coastal current northward, shoreward of the West Spitsbergen Current. Sea ice extent decreases northward, a clear indication that melting is taking place. The coastal current also advects the Arctic Water mass from its origin in Storfjorden and the Barents Sea. The two currents are illustrated in

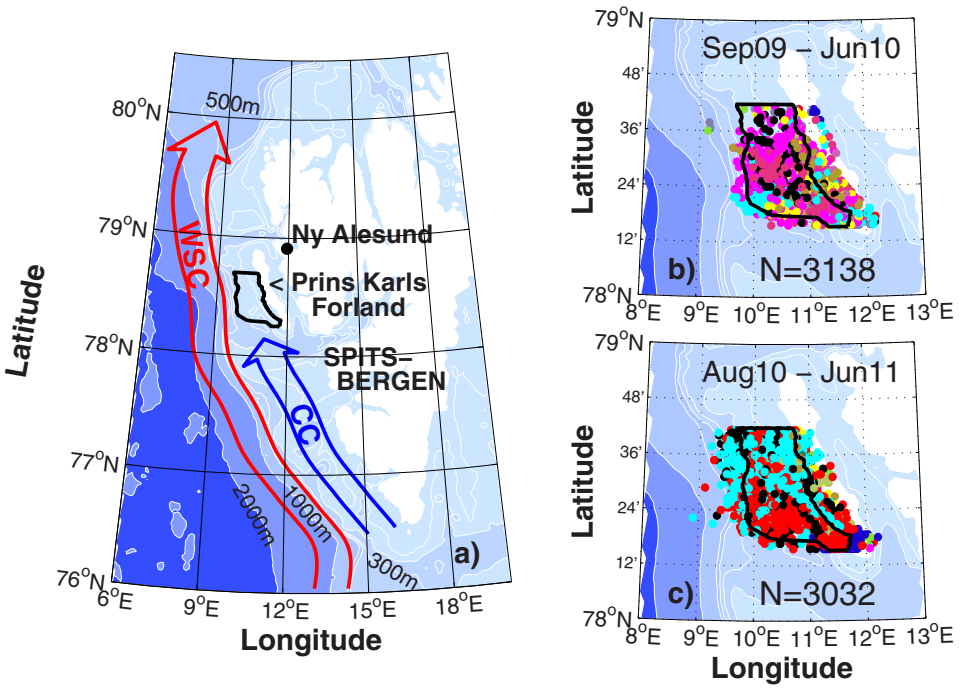

Figure 1. (a) Main current systems west of Spitsbergen; WSC = West Spitsbergen Current, CC = Coastal Current. Black line encircles model domain. (b) Positions of profiling dives made by 15 harbor seals during the period 1 September 2009 to 17 June 2010. (c) Positions of profiling dives made by 14 harbor seals during the period 24 August 2010 to 23 June 2011. N = number of dives.

Figure 1, along with positions of temperature and salinity profiles collected by harbor seals equipped with Conductivity-Temperature-Depth Satellite Relay Data Loggers (CTD-SRDLs—developed and built by the Sea Mammal Research Unit, University of St Andrews, Scotland) during two winters (2009–2011). In the present study, we utilize this unique data set to explore whether Atlantic Water-induced melting of the drift ice is important for the winter development of the water column in the geographical region of the West Spitsbergen Shelf, indicated in Figure 1.

Exchange between Atlantic Water in the West Spitsbergen Current and the shelf and fjord water along west Spitsbergen has been the subject of several investigations. For example, analyses of mooring data from this area indicate that lateral diffusion of heat from the West Spitsbergen Current can be substantial [*Nilsen et al*., 2006] and increased inflow of Atlantic Water on the shelf has been linked to upwelling events induced by northerly winds [*Cottier et al*., 2007]. In the *Tverberg and Nøst* [2009] idealized model study, eddy overturning was shown to be important for lateral exchange and could explain typical structures of the shelf edge front west of Spitsbergen. Eddy overturning evolves as a long-term mean effect of eddy activity that reduces available potential energy; it is an essential part of the residual-mean overturning as described by, e.g., *Marshall and Radko* [2003]. This residual-mean overturning acts in a plane perpendicular to a steady state geostrophic current and is the sum of an Eulerian mean overturning and eddy overturning; e.g., expressed as a stream function: $\Psi_{res}=\bar{\Psi}+\Psi^*$, where $\bar{\Psi}$ is the overturning stream function for the Eulerian mean flow and Ψ^* for the eddy overturning. A typical Eulerian mean overturning is wind-driven Ekman overturning. In the ocean interior, where there is no buoyancy forcing, the stream function of the residual flow is aligned with the isopycnals, and a residual overturning can be driven by buoyancy forcing in the surface mixed layer. *Marshall and Radko* [2003] deduced the following expression for a steady state residual stream function at the base h_m of the mixed layer:

$$\Psi_{res|z=-h_m}\frac{\partial b_0}{\partial x}=\widetilde{B}_0, \tag{1}$$

where $b_0(x)$ is the mixed layer buoyancy and $\widetilde{B}_0$ is the net buoyancy supplied to the mixed layer by air-sea buoyancy fluxes and possibly also by lateral diabatic eddy fluxes in the mixed layer. We have replaced their coordinate y with x to better fit the east-west alignment of the overturning across the West Spitsbergen

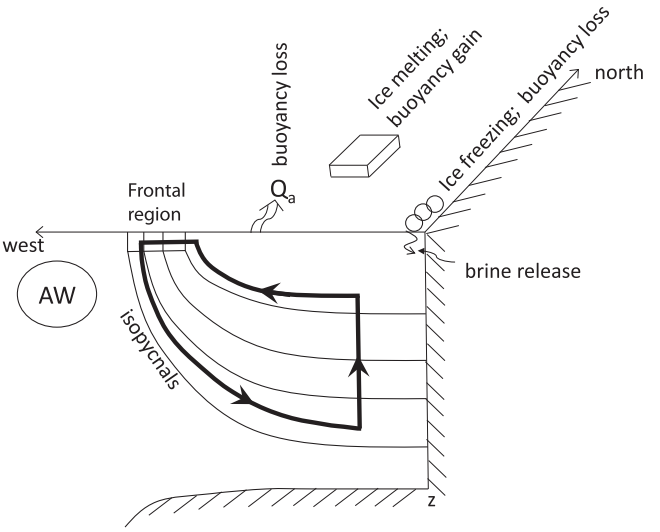

Figure 2. Conceptual model of processes that can change the properties of the water column on the shelf. Q_a is ocean-atmosphere surface heat flux. AW is Atlantic Water in the West Spitsbergen Current. The shelf is indicated with a bottom line, and the shore is to the right.

Current. Figure 2 illustrates a situation when the shelf edge front is a density front with warm, saline Atlantic Water being denser than the fresher and colder shelf water; possible buoyancy sources that could drive a residual overturning across the front are included. We also suggest a residual overturning from the simplest case when $\widetilde{B}_0$ is a steady negative buoyancy source, resembling winter heat loss to the atmosphere. From equation (1), the stream function at the base of the mixed layer is $\Psi_{res|z=-h_m} < 0$, because $\partial b_0/\partial x > 0$. This is equivalent to a residual flow toward the west (away from the coast), because the surface is a physical boundary for the flow, so $\Psi_{res|surface} = 0$. This overturning acts to put light water on top of denser water. Somewhere in the frontal zone, the mixed layer buoyancy gradient $\partial b_0/\partial x$ increases implying that $\Psi_{res|z=-h_m}$ becomes less negative and downwelling must occur. Alternatively, the same may happen if $\widetilde{B}_0$ weakens. The resulting residual overturning brings surface water into the frontal zone from the shelf area, where it mixes with the water there. This mixed water downwells into the deepest part of the shelf, where it is subsequently mixed upward in the water column. In the deep part of the shelf water column, one would then expect to find water with temperature/salinity characteristics falling along a mixing line between surface shelf water and Atlantic Water. Eddy-induced mixing in the frontal zone can be substantial according to *Marshall et al.* [2006], who estimated that straining and stretching of tracer fields by surface eddies in the Antarctic Circumpolar Current could increase the effective diffusivity to large values, up to 2000 or 3000 m^2/s.

Drift ice on the shelf will be caught in the residual-mean overturning (see Figure 2) and possibly melt in the frontal zone, or on the shelf itself due to upward mixing of warmer water. Sufficient melting will maintain the situation with shelf water being less dense than the Atlantic Water in the West Spitsbergen Current. In fact, if no drift ice is present on the shelf, residual overturning will eventually even out buoyancy differences across the front, and continued surface buoyancy losses on the shelf should result in dense water formation on the shelf. This situation will resemble overturning across the Antarctic shelf slope in regions where Antarctic Bottom Water is formed [*Stewart and Thompson*, 2013].

Drift ice melting in the frontal zone, combined with downwelling due to residual overturning, could create a cold halocline layer structured water column on the shelf (see Figure 2). We will search for evidence of such a process, though the main aim of our study will be more general. We seek to quantify the relative importance of processes that, in combination, transform the water masses on the shelf west of Spitsbergen. The paper is organized as follows: section 2 sketches the approach we have chosen and the research questions that arise; the seal data are introduced in section 3 and the heat and freshwater budget box model in section 4. Both sections 3 and 4 have supplementary information in Appendixes. In section 5, hydrography from the seal data is displayed along with box model results. A discussion of the results, including uncertainties, is given in section 6.

2. Research Questions and Approach

We have utilized observational data (temperature and salinity) collected by CTD-SRDL instrumented harbor seals (*Phoca vitulina*) that traveled and dived freely over the shelf west of Prins Karls Forland, to estimate the heat and freshwater content in a water body situated on the shelf of west Spitsbergen within the domain indicated in Figure 1. With a box model approach, we have then quantified the heat loss to the atmosphere, ice

freezing, and melting, and the inflow of Atlantic Water needed to explain the observed variation in heat and freshwater content in the shelf water. All these processes are summarized in Figure 2. Additionally, some northward advection in the coastal current on the shelf was specified in our model runs, as well as precipitation and evaporation. Two major research questions arose—first, whether it was Atlantic Water inflow or sea ice formation that was responsible for the decreasing freshwater content in the shelf water body during winter. Second—is the Atlantic Water inflow governed by wind-driven Ekman overturning or buoyancy-forced residual-mean overturning across the shelf edge front? In residual-mean theory, it is the combination of Ekman and eddy overturning; the residual-mean overturning that determines the water mass flow across the front. The overturning in the box model is formulated such that it fits both Ekman and eddy overturning. The seal data reveal that sea ice formation and melting can take place simultaneously within the shelf domain. The box model, however, selects one of these processes to be more influential in changing shelf water properties during each time step. The validity of these choices will be addressed during our discussion. Using this box model approach, we demonstrate that eddy overturning is the dominant part of the residual overturning that supplies warm Atlantic Water to the continental shelf during winter, and that this is a key process in determining variation in the heat and freshwater content of the shelf water column during winter.

3. Seal Data

Harbor seals were captured at Prins Karls Forland, on the west coast of Spitsbergen, and equipped with CTD-SRDLs. Fifteen adult/subadult animals were equipped with these tags in 2009 and 14 additional seals were instrumented in 2010 (N = 29 total). All ARGOS (http://argos-system.org) positions of profiling dives are shown in Appendix A, Figure A1 (N = 16,567 profiles), and the ones used in the present study are illustrated in Figure 1 (N = 6170 profiles). The seals made occasional dives in the West Spitsbergen Current, but most dives were between the front and the shore.

Some adjustments to the salinity and temperature data were necessary. This was done based on intercalibration between the different seals' tags. The calibration was done with the aid of TS diagrams, based on typical profiles taken during March and April, where surface temperature values were set to the freezing point and the deepest parts of the profiles were close to the typical temperature (3–4°C) and salinity (35.1) values for Atlantic Water in this region. Supercooling was allowed for in shallow profiles close to the shore. In accordance with previous treatments of similar data [*Nøst et al*., 2011], the adjustments, with one exception, were stable time constants for each instrument/seal. Details about the intercalibration method and adjustment constants for each instrument are given in Appendix A.

In the present study, only data from a restricted geographical area on the shelf just west of Prins Karls Forland (Figure 1) were used. The selected domain contained the densest data set (in time), and is considered small enough to contain CTD profiles with minimal north-south variation. Bottom depth data in the domain were extracted from IBCAO (International Bathymetric Chart of the Arctic Ocean). The southern boundary was set at 78.25°N and the northern boundary at 78.7°N, a distance of approximately 50 km. The 200 m isobath was selected as the western boundary of the domain. The average surface width of the domain is then approximately 30 km, and the total water volume is approximately 150 km^3. The average depth in this area is 140 m.

A hydrographic time series was constructed from the seal data within the selected domain, with some exceptions (outlined in Appendix A), and a smoothed version of this time series was constructed. The smoothing was a moving average within pressure bins and 14 day time periods. The pressure bins used were 5–10, 10–15, 15–20, 20–30, 30–40, 40–50, 50–60, 60–80, 80–100, 100–150, and 150–200 dbar. Daily profiles were constructed as follows: all observations made in a 14 day period in each depth bin were used to create an average value centered around each given day (following *Nøst et al*. [2011]). Sample sizes (number of data points) and standard deviations are presented in Appendix A. The smoothed time series were used as input to the heat and freshwater budget model.

4. Heat and Freshwater Budget Model

In order to quantify the contributions of the different processes to temperature and salinity variations in the shelf water column, a bulk budget model was developed for the geographical shelf domain (see Figure 1). The bulk budget model includes contributions from surface heat flux q_{surf}, net precipitation-evaporation F_{pe},

residual overturning (q_{res}, F_{res}) (the sum of Ekman and eddy overturning), sea ice melting (q_m, F_m) and freezing (q_{fr}, F_{fr}), and specified northward advection of Arctic Water in the coastal current on the shelf (q_{adv}, F_{adv}). The sum of these terms determines the observed temporal changes in heat content q_{vol} and freshwater content F_{vol} in the geographical domain:

$$\begin{aligned} q_{vol}(t+\Delta t)-q_{vol}(t)&=q_{surf}(t)+q_{res}(t)+q_m(t)+q_{fr}(t)+q_{adv}(t)\\ F_{vol}(t+\Delta t)-F_{vol}(t)&=F_{pe}+F_{res}(t)+F_m(t)+F_{fr}(t)+F_{adv}(t), \end{aligned} \tag{2}$$

where heat and freshwater contents are based on the smoothed seal data outlined in the previous section. They can be simplified to:

$$q_{vol}(t) = \bar{q}(t)\,\bar{W}\bar{h} \wedge F_{vol}(t) = \bar{F}(t)\,\bar{W}\bar{h}, \tag{3}$$

with little loss of accuracy, where $\bar{W} \approx 22$ km is a depth-averaged shelf width and $\bar{h} \approx 140$ m is the mean depth of the shelf domain. Mean heat and freshwater content of a water parcel on the shelf

$$\bar{q}(t) = c_{pw}\,\rho_w\,(\bar{T}(t)-T_f) \wedge \bar{F}(t) = \rho_w\,(S_{ref}-\bar{S}(t)), \tag{4}$$

is determined by mean temperature $\bar{T}(t)$ and salinity $\bar{S}(t)$ values, which are shelf width-weighted and depth-integrated averages of the smoothed seal data profiles. The values of specific heat c_{pw}, density ρ_w, and freezing point temperature T_f are set to correspond to the mean values of temperature $\bar{T}(t)$ and salinity $\bar{S}(t)$. Details of the averaging procedure as well as each of the terms in the budget model (equation (2)) are presented in Appendix B. Here, a brief overview of the formulation of the different terms is given. The forcing terms in equation (2) are positive when they heat/freshen the shelf water body. Heat flux Q_a (J s^{-1} m^{-2}) through the ocean surface only penetrates the open water fraction $(1-a)$ of the domain, and must be integrated across the north-south average of the surface width of the domain; $W(0)$. During every time step, heat is added/subtracted through the surface according to

$$q_{surf}(t) = [1-a(t)]\,Q_a(t)W(0)\,\Delta t, \tag{5}$$

where Δt is one time lapse (1 day). This surface flux term is specified from bulk formulae [*Renfrew et al.*, 2002] and sea ice cover data. See Appendix B for more details.

In the formulation for the residual overturning (q_{res}, F_{res}) across the shelf edge front, we assume that Atlantic Water on the ocean side of the front remains denser than the shelf water throughout the modeled time period. We then assume that the most common overturning direction will be as shown in Figure 2, and analogous to an overturning induced by surface Ekman transport toward the west, i.e., away from the coast. This overturning is defined to be negative, bringing Atlantic Water (q_{aw}), containing no freshwater, onto the shelf and surface characteristics (q_s, F_s) of the shelf water out of the domain:

$$q_{neg}(t) = U_{neg}(t)\,[q_s(t)-q_{aw}(t)]\,\Delta t \wedge F_{neg}(t) = U_{neg}(t)\,F_s(t)\,\Delta t, \tag{6}$$

with its residual volume flux (pr north-south meter) U_{neg} (m^2 s^{-1}) being negative. We assume that this overturning advects sufficient surface shelf water into the surface layer of the West Spitsbergen Current, that an occasional reversed overturning will bring this surface shelf water (q_s, F_s) back onto the shelf and deep shelf water (q_b, F_b) out of the shelf domain:

$$q_{pos}(t) = U_{pos}(t)\,(q_s(t)-q_b(t))\,\Delta t \wedge F_{pos}(t) = U_{pos}(t)\,(F_s(t)-F_b(t))\,\Delta t, \tag{7}$$

and the residual volume flux (pr north-south meter) U_{pos} (m^2 s^{-1}) here is positive. The residual overturning (q_{res} and F_{res}) in equation (2) is a choice between positive or negative:

$$q_{res}(t) = \delta q_{pos}(t)+(1-\delta)q_{neg}(t) \wedge F_{res}(t) = \delta F_{pos}(t)+(1-\delta)F_{neg}(t), \tag{8}$$

where the delta function δ is either 0 or 1. The residual volume flux (U_{neg} and U_{pos}) has similar dimensions to the surface Ekman volume transport in an east-west direction:

$$U_x^{ek}(t) = \frac{\tau_y(t)}{\rho_w f}, \tag{9}$$

where τ_y is wind stress in a north-south direction, ρ_w is density of sea water, and $f = 1.43 \times 10^{-4}$ s^{-1} is the Coriolis parameter, which would be the Eulerian mean part of the residual overturning.

The sea ice melting terms (q_m, F_m) are formulated as

$$q_m(t) = d_m(t)\rho_i L_i W(0) \wedge F_m(t) = d_m(t)\rho_i(S_i - S_{ref})W(0), \tag{10}$$

where the model tuning parameter d_m is negative, so the volume (per m of shoreline) of sea ice that melts during each time step in the model domain is $-d_m W(0)$. The density of sea ice $\rho_i = 917$ kg m^{-3} and latent heat of fusion $L_i = 2.67 \times 10^5$ J kg^{-1} were set as simple constants, analogous to *Boyd and D'Asaro* [1994], corresponding to sea ice temperature -5°C and salinity $S_i = 7$ psu. The sea ice freezing terms (q_{fr}, F_{fr}) are formulated as

$$q_{fr}(t) = d_{fr}(t)\rho_i L_i W(0) \wedge F_{fr}(t) = d_{fr}(t)\rho_i(S_{ifr} - S_s)W(0), \tag{11}$$

where the model tuning parameter d_{fr} (m) is the thickness of sea ice formed during the model time step Δt (1 day), averaged over the model domain surface width $W(0)$. S_{ifr} is the salinity of newly formed sea ice and S_s is surface salinity extracted from the seal data.

The model also includes a specified advection term for Arctic Water in the coastal current:

$$q_{adv}(t) = U_{arw}(t)\,(q_{arw} - \bar{q}(t))\,\Delta t \wedge F_{adv}(t) = U_{arw}(t)\,(F_{arw} - \bar{F}(t))\,\Delta t, \tag{12}$$

where $U_{arw} \approx (0.3$ m^2 s$^{-1})$ is a specified volume flux of Arctic Water (q_{arw}, F_{arw}). See Appendix B for details on choices of parameter values. The precipitation-evaporation term is an order of magnitude smaller than the other terms, and is only described in Appendix B.

Our problem (equation set 2) contains altogether four tuning parameters: U_{neg} (equation (6)), U_{pos} (equation (7)), d_m (equation (10)), and d_{fr} (equation (11)). However, the overturning cell is either positive or negative, and it is assumed that during each time step there is either ice melting or freezing. Consequently, a balance between two processes occurs in each time step, and the heat and freshwater budget model equations can be explicitly solved since only two unknowns appear. Four combinations are possible: (1) negative overturning (Atlantic Water entering the domain at depth) and melting ice (U_{neg} and d_m); (2) negative overturning and ice freezing at the surface (U_{neg} and d_{fr}); (3) positive overturning and ice melting (U_{pos} and d_m); or (4) positive overturning and ice freezing (U_{pos} and d_{fr}). Detailed description of the solution method we selected with error estimates is given in Appendix C.

5. Results

Intercalibrated temperature and salinity data are plotted in TS-diagrams in Figure 3. The plots are separated temporally, at approximately the time when the surface heat flux switches from cooling the water column to heating the water column. This happened earlier in the spring of 2011 compared to 2010. Standard characteristics of Arctic Water are indicated in the figure to show that a large portion of shelf water at the end of the winter season shows these characteristics. Figure 4 displays some of these same observations from selected 14 day time periods. The observations from each period are plotted on top of the smoothed version of the time series in which the observations are averaged in pressure and time bins. The smoothed data are presented as Hovmöller diagrams in Figure 5. The data show that water close to Atlantic Water characteristics is most of the time present in the deep part of the shelf water column (see both Figures 4 and 5). The surface water is gradually transformed from a fresh water mass to a gradually colder and more saline one during both winters. In the TS diagram, most of the observations fall on a mixing line between this surface water and Atlantic Water characteristics. Some observations also fall along the freezing line. Among these, the observations that are less saline than the coldest water along the mixing line we interpret to be the result of sea ice melting, and the observations that are more saline we interpret to be brine enriched water from sea ice formation. The observations colder than the freezing line are the result of supercooling in shallow areas close to the shore. Time series of additional input data to the box model; daily values of surface heat flux Q_a as well as daily values of ice cover fraction a, are shown in Figure 6 (used in equation (5)).

Time series of the box model's estimated tuning parameters (overturning strength ($U_{neg} + U_{pos}$) and daily ice thickness melting, and formation ($d_m + d_{fr}$) from equations (6), (7), (10), and (11) are shown in Figure 7. Each estimate varies over a range determined from the error estimates. Ekman transport, calculated from equation (9), is plotted along with the modeled overturning. The heat and salt fluxes associated with overturning and ice melting/freezing are shown in Figure 8, along with surface heat flux modified by the amount of ice

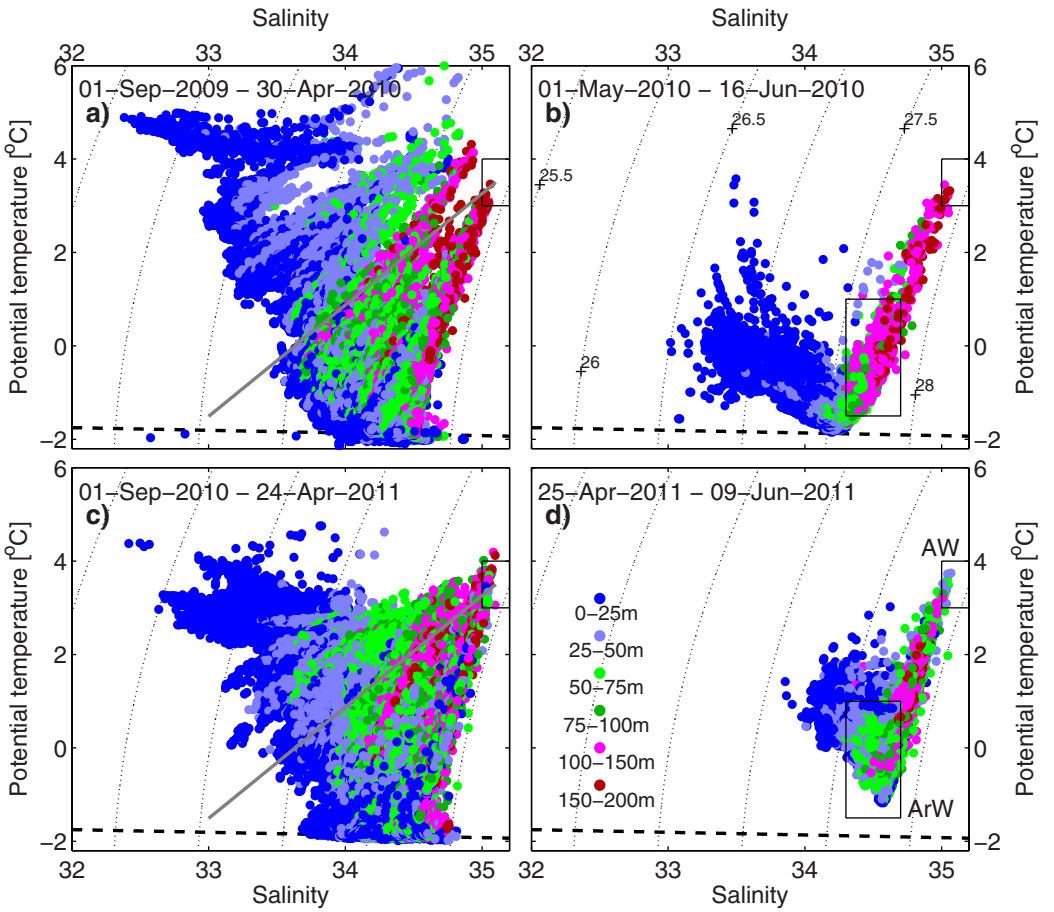

Figure 3. TS diagrams using observations from within the geographical domain in Figure 1 from the 2009–2010 and 2010–2011 seasons, separated at the onset of the melting seasons within each sampling season. Dotted, curved lines are isolines of potential density. The black rectangles indicate two water types: Arctic Water (ArW) (typically with summer characteristics ranging T = (−1.5 to 1)°C and S = (34.3 to 34.7)) and Atlantic Water (AW) (with winter characteristics typically ranging from T = (3–4)°C and S = (35–35.2)). Black dashed line is the freezing line. Gray line is the melting line, when sea ice of 7 psu is melted in Atlantic Water.

cover present (see equation (5)) and observed heat and salt changes (dq and dS) transformed from equation (2). Error ranges arising from the standard deviation of the heat and freshwater content are included. Mismatches in the tuning of the heat budget (red bars in plots a and c) could be attributed to heat conduction through the ice, or to errors in prescribed surface heat flux estimates. The extra heat loss needed in each of these episodes is also added to the surface heat flux time series, Figure 6.

Since eddy overturning is a long-term effect, for which daily estimates are not really realistic, the modeled results are averaged over time. The two winter seasons are divided into a total of five periods, and mean values of overturning and ice melting/freezing for each period are given in Table 1. The early part of the winters (periods i) is characterized by weaker overturning than the later parts of the winters (period iii in 2010 and period ii in 2010/2011). In order to get a sense of how dominating the overturning and melting processes are, tentative time evolutions for temperature and salinity, governed by only parts of the modeled terms, are shown in Figure 9. The first scenario accounts for residual overturning (U_{res}) combined with melting (d_m) and surface heat flux to the atmosphere (q_{surf}). The second scenario describes when advection of Arctic Water (U_{arw}) in the coastal current is incorporated in addition. The mismatch between the latter curves and the curves of observed mean temperature and salinity are then attributed to sea ice freezing and excess heat loss or brine release.

6. Discussion

The heat and freshwater budget box model created herein suggests that Atlantic Water melting drift ice, in combination with surface heat flux to the atmosphere, are the dominant processes that capture most of the

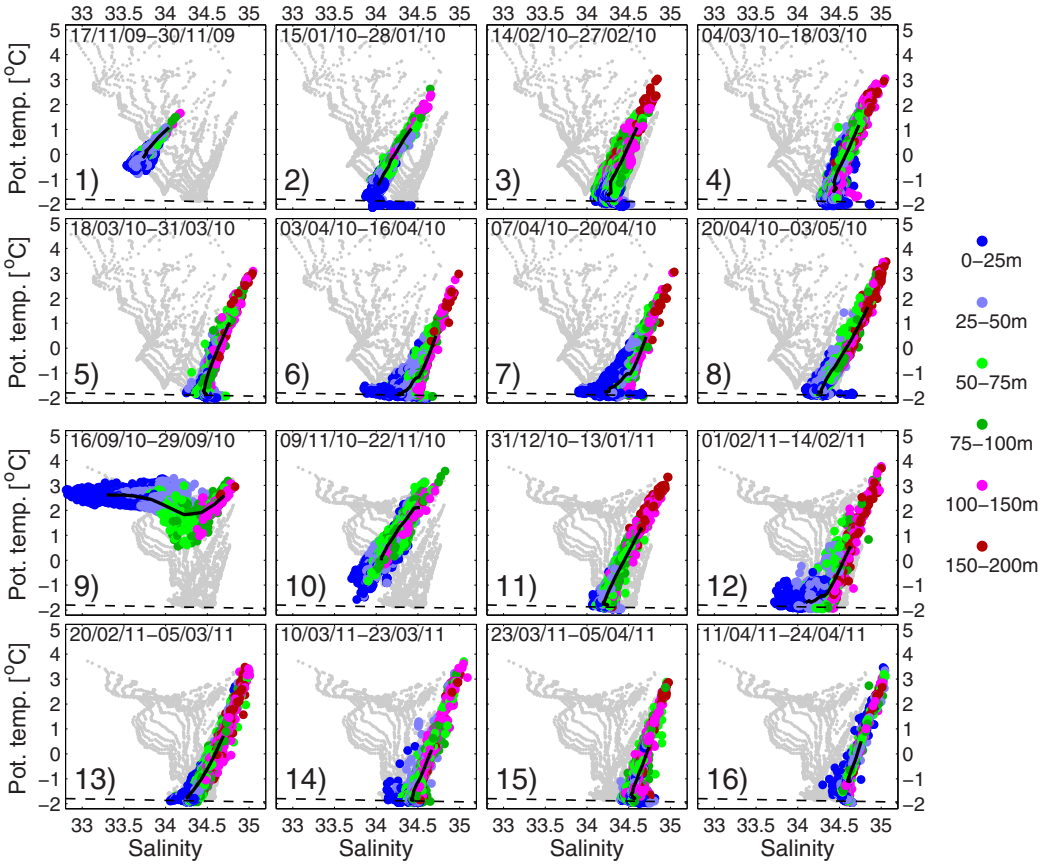

Figure 4. TS diagrams of original observations from selected 14 day periods from Figure 3. Gray dots: 14 day moving average values up till 30 April 2010 and 24 April 2011. Black solid lines indicate the moving average profiles centered in each 14 day period (displayed in Figure 5). Black dashed line is the freezing line.

variability in mean temperature and salinity observed during winter in the shelf domain (west of Spitsbergen). There is a general increase in salinity of the shelf water during the winter (see Figure 9). However, it is not large enough to be explained purely by Atlantic Water exchange or sea ice formation. In the model tuning process, Atlantic Water exchange is usually selected in favor of sea ice formation. This is because, if ice freezing releases the same amount of heat as is added by this Atlantic Water exchange, ice formation would lead to stronger increases in the salt content, as long as newly formed sea ice has a salinity content larger than 10 psu.

6.1. Overturning

Traditionally, Ekman transport has been suggested to be the main driving mechanism for cross-frontal exchange. And in fact, the time step we use (1 day) is better suited to describe Ekman overturning than eddy overturning. Eddies can mix and unmix on a day-to-day time scale, and will induce a mean overturning only over a period of weeks. It is therefore interesting to compare whether variations in Ekman transport are reflected in the modeled residual overturning. The strength of the modeled residual overturning U_{neg} and U_{pos} is comparable to Ekman transport calculated from the wind stress (see Figure 7). It is clearly biased toward negative overturning, which is also the dominant Ekman overturning (off-shore Ekman transport due to northerly winds). During the first winter, the correlation between estimated overturning and the Ekman transport is statistically significant, and explains 17% of the variation in the time series of daily values (correlation coefficient $R = 0.41$ with p value $<1\times10^{-3}$, 43 degrees of freedom). The correlation increases slightly when the time series are low-passed-filtered with a 14 day time window. The correlation becomes very high ($R = 0.77$ with p value $<1\times10^{-3}$, 8 degrees of freedom) when a time lag of 6 days between the time series is introduced, with residual overturning leading Ekman transport. Such a time lag is however difficult to interpret (see the following). The residual overturning time series from the second winter is not significantly

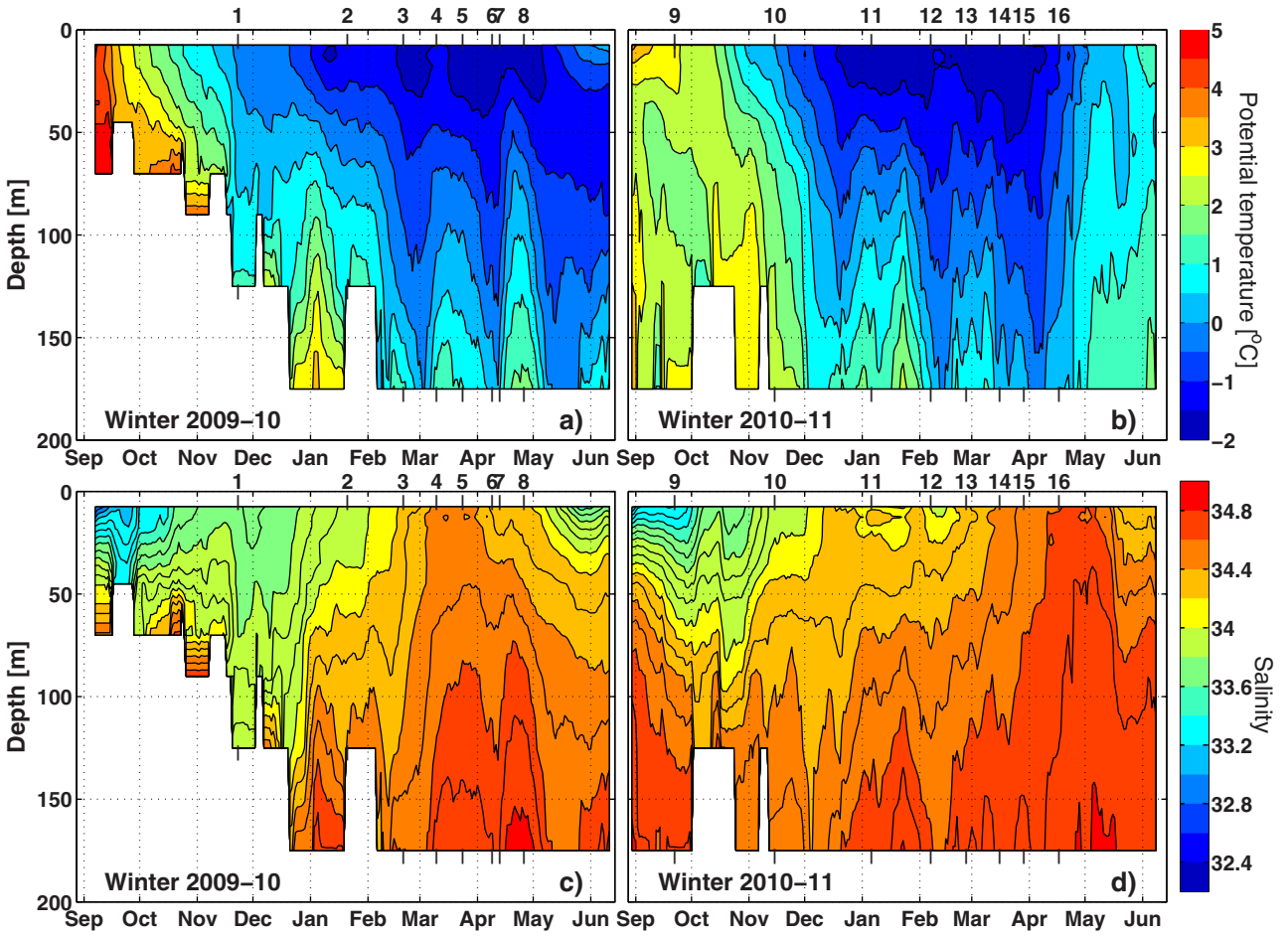

Figure 5. (a and b) Temperature and (c and d) salinity from 2009–2010 and 2010–2011 averaged in depth and time bins with data from within the geographical domain in Figure 1.

correlated with Ekman transport (R = 0.15 and *p* value = 0.06). We interpret the difference between the two winters as an effect of the nature of eddy overturning. Ekman transport can trigger eddy formation. However, the eddy overturning will always tend to flatten isopycnals (i.e., put lighter water on top of denser water, see, for instance, *Marshall et al*. [2002]). When both processes act in the same direction (e.g., northerly winds combined with buoyancy forcing) both processes can be involved with the overturning. However, we would then expect Ekman to lead eddy overturning. Onshore Ekman transport due to southerly winds can lead to a sharper shelf edge front and more eddy formation caused by baroclinic instabilities, and a sharp front will be linked to downwelling in the frontal zone, according to steady state residual theory (see equation (1)). During February 2011, the modeled overturning was negative, overriding the Ekman overturning, and inducing ice melting (see Figure 7). Ice cover decreased during that period (see Figure 6), from 50% to 20%. Moreover, the Atlantic Water did not seem to enter the shelf in the surface as an on-shore Ekman transport would force it to do (see Figures 4 and 5). The more frequent incidents of southerly winds in the winter of 2010–2011 compared to 2009–2010 may thus be the reason for the lower correlation between residual overturning and Ekman transport observed in the second year of our study. We conclude that the eddy overturning decides the direction of the residual overturning.

6.2. Cold Halocline Layer Formation

Taking a closer look at the original seal data, February 2011 proves to be particularly interesting; we observed an occurrence of cold halocline layer profiles (close to freezing temperature and stratified in salinity), which appear to be associated with drift ice melting. A similar occurrence was also observed the first winter, and salinity and potential temperature profiles from both incidents are displayed in Figure 10 along with two occurrences apparently associated with sea ice formation. The profiles from the same dates are

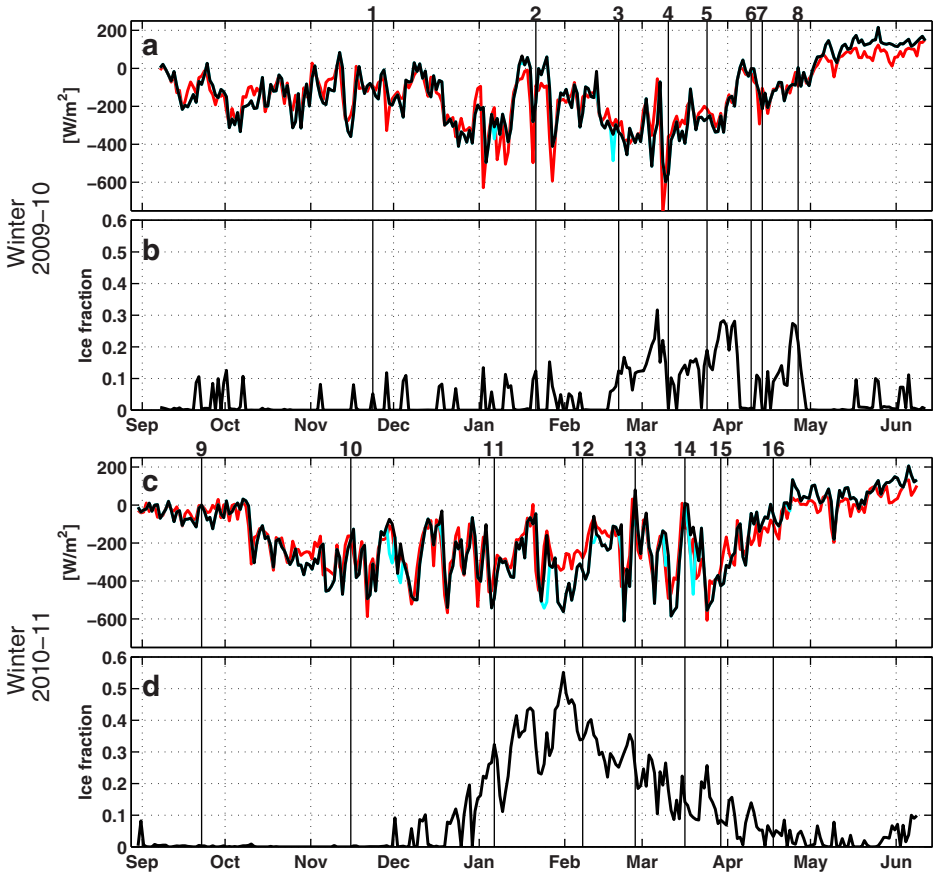

Figure 6. Environmental data from the two winters 2009–2010 and 2010–2011: (a and c) surface heat flux (positive downward) in black (empirical formula) and red (ERA-Interim data at a position centrally in the model domain; 78°30′N and 10°30′E). Blue lines: episodes of excess heat loss suggested by model estimated ice formation. (b and d) Sea ice fractions averaged inside the box defined by 78°18′N–78°36′N and 10°E–11°E. Numbered vertical lines indicate dates centered in the 14 day clustered TS plots shown in Figure 4.

viewed in TS diagrams in Appendix A, Figure A5, plots 5 (24 March 2010), 6 (9 April 2010), 12 (7 February 2011), and 15 (29 March 2011). Figure 4 indicates that melting is taking place during the 14 day periods centered around the dates of Figure A5, plots 6 and 12, but not plots 5 and 15. According to the model results, the cold halocline layer occurrences associated with melting (plots 6 and 12) are preceded by a period of strong melting and relatively weak overturning (Figure 7), and the environmental data indicate strong surface heat loss and rapid melting (Figures 6c and 6d) as well as southerly winds (Figure 7). Model results are not so clear for the cold halocline layer occurrences associated with sea ice formation, but they also appear to be preceded by southerly winds and strong surface heat loss. These episodes, both associated with melting and freezing, appear to be fairly rare. However, there are additional cases where deep profiles homogeneous in both temperature and salinity are formed, apparently associated with both ice melting and freezing. Quite soon after all these incidents new mixing lines are formed in the TS diagrams between less saline or more saline surface water and Atlantic Water (this is difficult to show in figures, but indications can be seen in Figure 4, plots 4, 6, 12, 14, and 15), when surface water is apparently mixed downward in the water column.

The residual overturning process (Figure 2) can explain how melt water is brought down in the water column when ice melts in the frontal zone; forming a cold halocline layer. It can also explain why the profiles return to the typical state so quickly, where most of the salinity and temperature data points are aligned along the mixing line between Atlantic Water and shelf water. When ice melts in warm water, there is also an additional process that might be considered; the characteristics of a water mass formed by warm water melting sea ice would fall along a melting line defined by equation (C4) (and indicated in Figure 3 if pure Atlantic Water was to melt sea ice of salt content 7 psu). However, as suggested by *Sirevaag and Fer* [2009], sea ice melting in combination with surface heat loss will form a melt water mix that is colder; such water

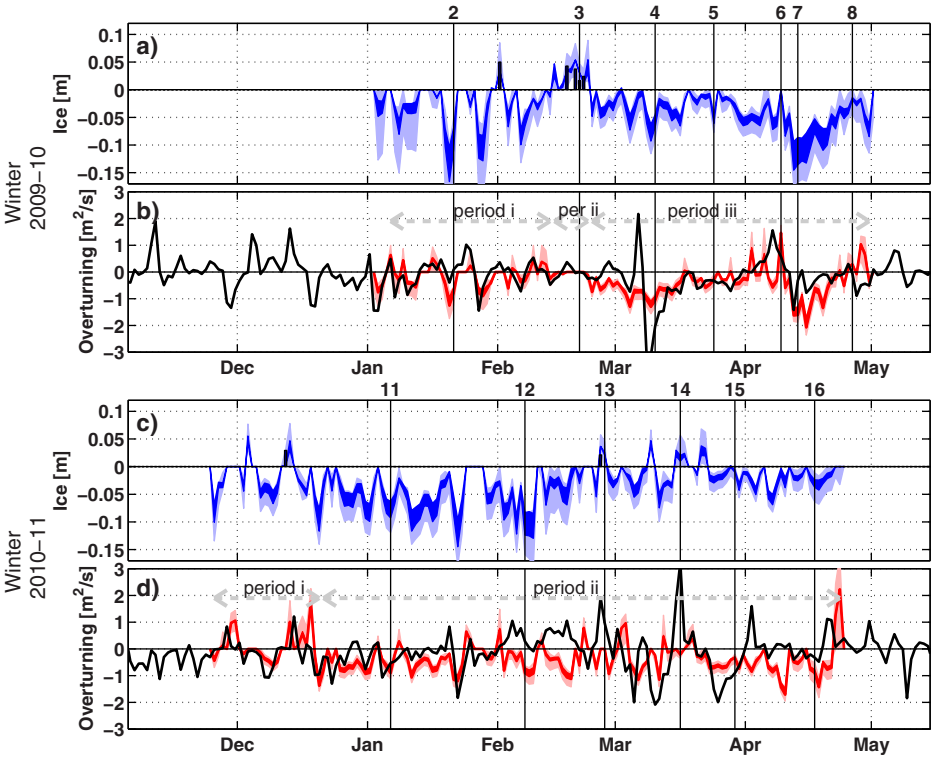

Figure 7. (a and c) Model tuned parameters of daily ice freezing plus ice melting (blue color). Black bars indicate extra salt (brine rejection) that has to be added to fit the model to the observed salinity changes. (b and d) Model tuned daily overturning (red color) compared with theoretical Ekman transport (black lines). For all plots, light colors show uncertainties arising from standard errors in seal data. Lower range in dark colors arise from 5 psu fresher sea ice (dark blue, Figures 7a and 7c) and 0.5°C warmer Atlantic Water (dark red, Figures 7b and 7d).

would fall along a steeper line in the TS diagram, and can even lead to an unstable water column and convection. This process could form cold halocline water away from the frontal zone, which also must be the case for cold halocline water formed by sea ice formation. The observations indicate that most of the ice freezing takes place in shallow areas close to shore (not shown).

6.3. Densest Water Formation

The continuous exchange of Atlantic Water in the West Spitsbergen Current combined with surface heat loss can explain how the stability of the shelf water column is gradually reduced by making the surface shelf water both colder and more saline. It is possible that ice formation contributes significantly to this destabilization, even though its contribution is small in the total budget. The presence of melting drift ice overall works against such an evolution and prevents the shelf water from becoming denser than Atlantic Water in the West Spitsbergen Current. The end product, as seen in both winters of this study, is a water type with characteristics close to the classic definition of Arctic Water with a salinity range 34.3–34.7 (Figure 3). In 2010, the shelf water column with lowest stability appeared in early March and the mixing line stayed more or less in the same position in the TS diagram throughout the month (see Figure 4, plots 4 and 5). This was also the period when a brine enriched water column was observed frequently, even though the model results suggest that melting was more influential. Melting intensified in April and made the water column slightly more stable. In 2011, the shelf water column with lowest stability appeared a bit later in March. However, it became even less stable than in 2010, actually almost homogeneous, and the mixing line in the TS diagram stayed in the same position throughout both March and April (see Figure 4, plots 15 and 16). In this period, the model also suggested that melting was important. However, the homogeneous water column implies that the shelf water had the same density as Atlantic Water in the West Spitsbergen Current. The front was no longer a density front, and the residual overturning would be different than assumed in the model. Both the Hovmöller diagram (Figure 5b) and the mean time series (Figure 9c) show that, throughout April, warming was taking place at the same rate at all depth levels in the shelf water column. The original profiles indicate that

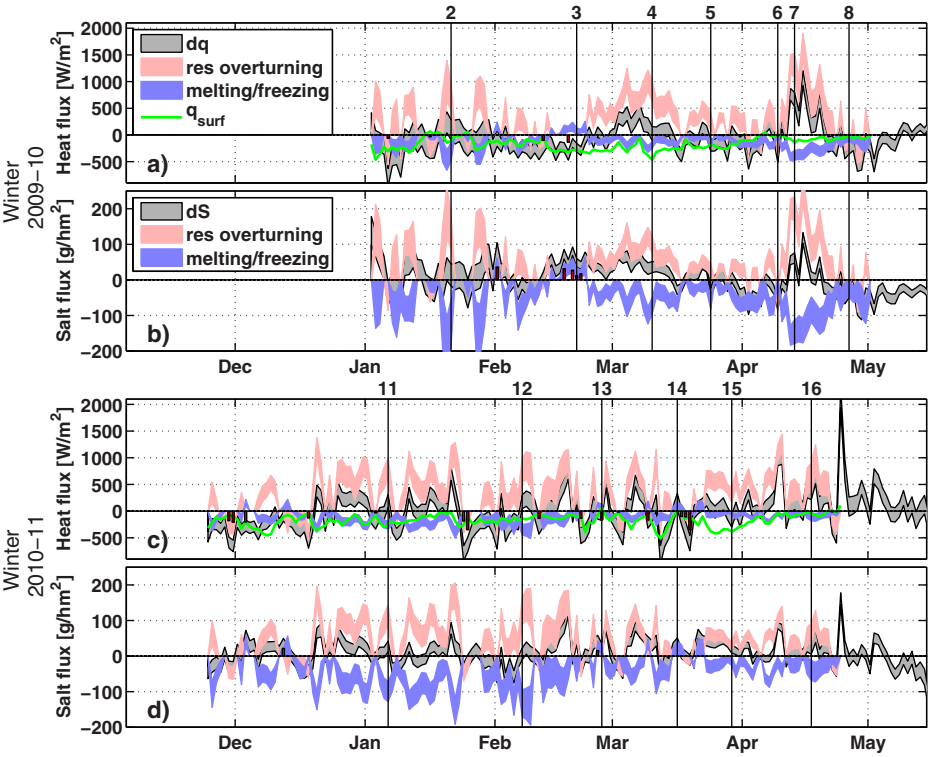

Figure 8. (a and c) dq; time step changes observed mean heat content, scaled to heat flux per second equivalents (left-hand side of equation (2) divided by $[W(0)\Delta t]$). (b and d) dS; time step changes in observed mean salinity content, scaled to brine release salt flux per hour equivalents (left-hand side of equation (2) divided by $[-24W(0)]$) [*Notz and Worster*, 2008]. Pink ranges are heat and salt fluxes due to model tuned residual overturning. Blue ranges are heat and salt fluxes associated with model tuned sea ice melting and freezing. Green lines in Figures 8a and 8c are specified surface heat flux q_{surf}, adjusted for open ocean fraction. All ranges arise from standard deviations in the observations. Red bars refer to mismatches in the salt budget (brine rejection) or heat budget.

some type of vertical overturning must have been involved, since points along the mixing line appear to originate from any depth during this period (see Figures 4 and A5).

In fact, the characteristics of the deepest water on the shelf can fall on any point along the mixing lines during these periods both in 2010 and 2011. In Figure 11, we show all data deeper than 100 m during the period between the first and the last observation of surface temperature lower than -1.5°C. It appears that melting and freezing, together with Atlantic Water exchange, are involved in a delicate balance keeping the shelf surface water at a salinity close to 34.7. A cold water mass with higher salinity than 34.7 would in fact be denser than Atlantic Water. When there is not sufficient ice melting, salinity of the shelf water may increase above this value, and it is likely to disappear from the shelf as a dense water plume that would descend down the continental shelf slope. This situation might have arisen at the very end of the winter period in 2010–2011 (25 April), when a sudden large jump in both heat and salt content was seen on the shelf (Figure 8). At that point in time, there had been fairly low concentrations of drift ice on the shelf for several days (Figure 6). In the Hovmöller diagrams (Figure 5) of smoothed temperature and salinity, cold

Table 1. Mean Magnitudes of Model Tuning Parameters: Ice Formation d_{fr} (Equation (11)), Melting d_m (Equation (10)), and Overturning $U_{res} = U_{neg} + U_{pos}$ (Equations (6) and (7)) During Selected Periods[a]

Period		d_{fr} (cm)	d_{frl} (cm)	d_m (cm)	U_{res} (m^2 s^{-1})	U_{arw} (m^2 s^{-1})
Period i 2010	6 Jan to 12 Feb 2010	0.1	0.1	−3.5	−0.15	0.3
Period ii 2010	13 Feb to 22 Feb 2010	3.1	1.3	0	0	0.3
Period iii 2010	23 Feb to 30 Apr 2010	0	0	−5	−0.45	0.3
Period i 2011	25 Nov to 20 Dec 2010	0.4	0.1	−3	0.05	0.3
Period ii 2011	20 Dec 2010 to 24 Apr 2011	0.2	0	−4	−0.4	0.3

[a]The parameter d_{frl} is interpreted as excess brine release from newly formed sea ice. Advection of Arctic Water U_{arw} (equation (12)) is specified in the model.

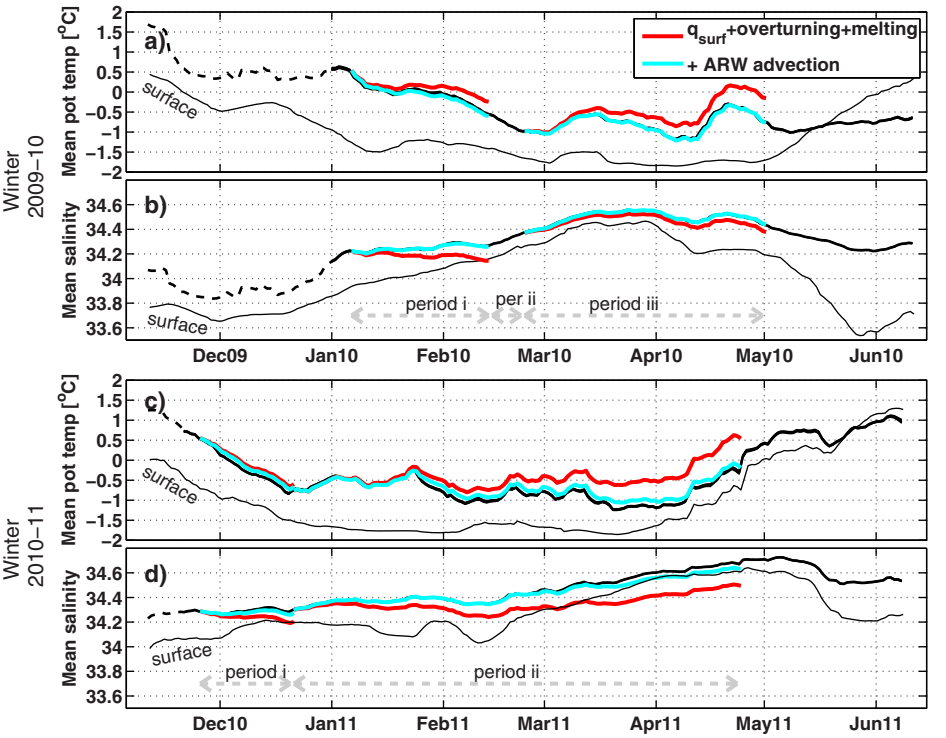

Figure 9. (a and c) Black curves are mean values of observed potential temperature and (b and d) analogous salinity (equation (B3)), from 2009–2010 to 2010–2011 within the geographical domain in Figure 1. The dashed part of the curves corresponds to periods when mean values are uncertain because deep profiles are lacking. Periods refer to Table 1. Red curves are modeled evolution of mean potential temperature and salinity due to surface heat flux (q_{surf}), residual overturning, and sea ice melting. Cyan curves include the same, but also advection of Arctic Water. Discrepancies of cyan from black curves are attributed to sea ice freezing and excess heat flux.

and relatively saline water near the bottom are suddenly replaced by typical Atlantic Water. There are very few seal dives during that period (the last few days of April 2011, see Figure A3), which may indicate that the environmental conditions were unfavorable for feeding.

When the area west of Spitsbergen is ice free, our results suggest that eddy overturning, in combination with surface heat loss, becomes the dominant process. The shelf water becomes more and more saline while remaining colder than the core of the Atlantic Water in the West Spitsbergen Current. This situation

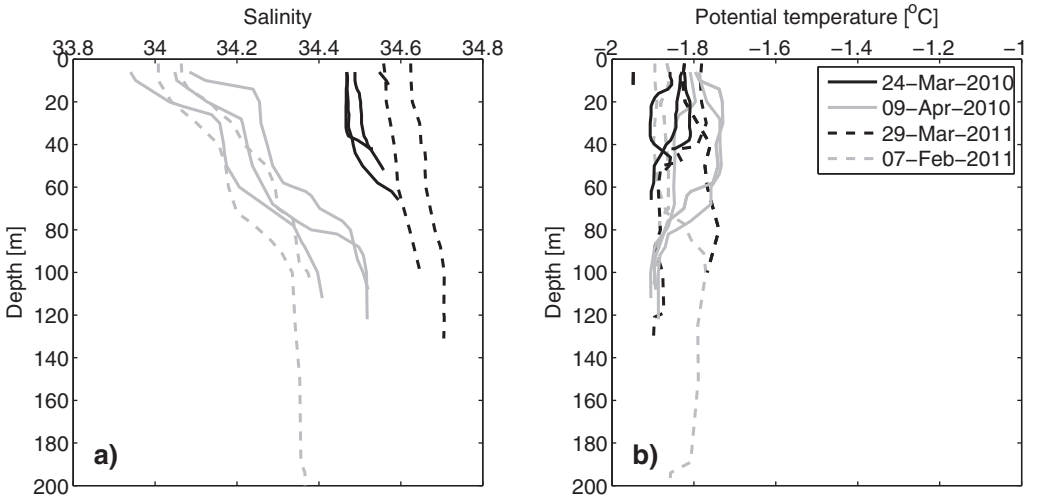

Figure 10. Selected profiles of (a) salinity and (b) potential temperature that resemble typical structure in the cold halocline layer; stratified in salinity and homogeneous, close to freezing temperature.

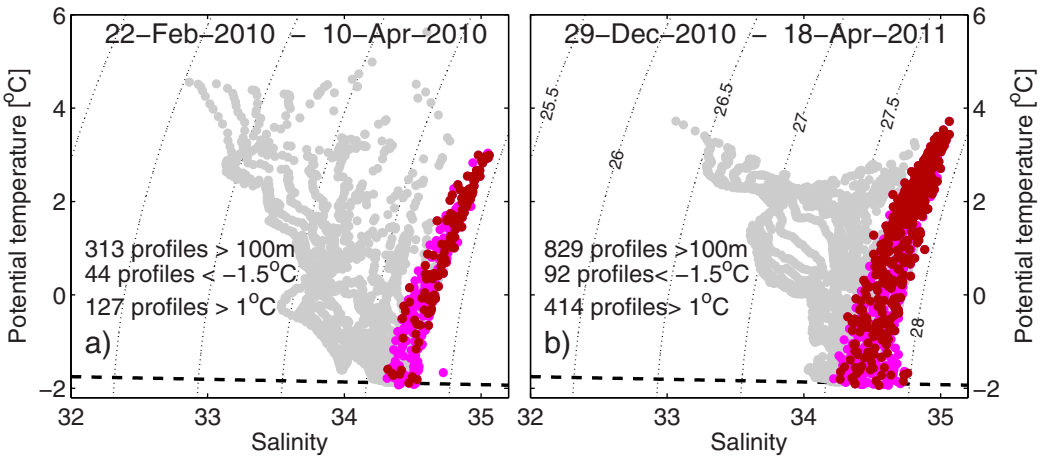

Figure 11. TS diagrams highlighting the deepest observations in profiles that are deeper than 100m and time limited between first and last observations of surface $T < -1.5^{\circ}$C are plotted. Gray dots: 14 day moving average values between 1 September and the onset of the melting season (30 April 2010 and 24 April 2011).

would eventually lead to a shelf water mass that is denser than the Atlantic Water and create a reversed eddy overturning with Atlantic Water entering the shelf near the surface. A situation with such reversed eddy overturning was observed in 2007 [*Tverberg and Nøst*, 2009], when a record minimum in the Arctic sea ice coverage (until that time) occurred. Ice conditions on the shelf also appear to have consequences for the strength and timing of the phytoplankton spring bloom in the region, as shown by *Hegseth and Tverberg* [2013], who used residual overturning to explain year to year variations.

6.4. Uncertainties

A question arises as to how realistic the modeled fluxes and tuning parameters are? Melting rates around 10 cm/d have been observed in the Marginal Ice Zone north of Spitsbergen under conditions with relatively warm water combined with strong surface heat flux [*Sirevaag*, 2009]. Most of the time, our model estimated melting rates are below 10 cm/d, or 10 cm/d is within the uncertainty range. According to *Notz and Worster* [2008] a reasonable ice thickness growth during 1 day is around 5 cm, which is also within the uncertainty range estimated by the model. Sometimes the inaccuracy in daily change in heat and freshwater content in the shelf domain makes it impossible to select which processes are most important. However, the number of days when only Atlantic Water inflow and sea ice melting can explain the changes is so numerous that in the total picture, this process combination overrides all other possible combinations (see Figure A6). The interested reader can compare the observed profiles in Figure A5, from 16 selected dates, with modeled parameters; these dates are marked in several of the time series figures (Figures 5–8).

The peak values of heat supplied by our model estimated residual overturning are generally larger in magnitude than the surface heat loss to the atmosphere. However, the variability is also large, so during the five periods with mean values of modeled overturning fluxes given in Table 1, the average heat supplied by the overturning is more moderate, amounting to 145, 20, 400, 90, and 360 W m^{-2} in each of the periods (i-2010, ii-2010, iii-2010, i-2011, and ii-2011), respectively. The mean heat loss to the atmosphere during each of these periods amounts to −150, −300, −190, −235, and −190 W m^{-2}, respectively, and is of the same order in magnitude. Errors in the prescribed surface heat flux can then over time be a significant error in the model. Air temperature and cloud cover data used in the empirical formula for surface heat flux were collected from a weather station on land, in Ny Ålesund, about 50 km east of the location of the model domain in Kongsfjorden. These air temperatures are likely to be somewhat colder, and cloud cover somewhat lighter than over the model domain, with the implications of stronger heat loss due to longwave radiation compared to the study domain. Wind data were extracted from ERA-Interim data [*Dee et al.*, 2011] from off the shelf, where they are stronger than inland. These data in combination, suggested that heat loss through the surface of the domain might be exaggerated by the empirical formulation. Comparisons between the surface flux used to force the model and surface fluxes extracted from ERA-Interim data (see Figure 6) indicate that this may be the case particularly during the 2010–2011 season. They are more similar

during the 2009–2010 season. However, during the second year of the study, there were more incidents when the cooling of the water column was stronger than can be explained by the surface heat loss, contradicting the suggestion that the empirical formula predicts an excessive surface heat loss. The interpretation that heat conduction into the ice plays a role during that winter is perhaps more realistic, as the ice cover is clearly denser during the second winter compared to the first. We chose to use an empirical formula rather than ERA-Interim fluxes directly, because we expect the ERA-Interim fluxes to be corrupted by the proximity to the West Spitsbergen Current. In fact, the ERA-Interim fluxes extracted from a location centered on the shelf domain are not able to provide the cooling observed in the shelf water column in the early phases of the winters (period i-2010 and i-2011 in Table 1).

Advection of Arctic Water in the box model was set to be rather weak (1 cm s^{-1}) and constant, with a resulting volume flux of 0.3 m^2 s^{-1}, which is comparable to the modeled residual overturning in strength. Test runs with stronger advection of Arctic Water produced stronger Atlantic Water overturning and ice melt, while test runs with weaker values gave slightly weaker Atlantic Water overturning and less ice melting (i.e., ice formation increased). However, incidents when excess cooling had to be accounted for also increased. In an eddy-rich current, a propagation speed of 1 cm s^{-1} is actually fairly realistic. In light of the strong lateral exchange across the shelf edge front that the box model results suggest the Arctic Water should perhaps not be defined as a specific water mass since both its freshwater and heat content depend on exchange magnitudes upstream of the model region. We attempted to control for this by keeping advection to a minimum as a compromise; we do not know the water characteristics on a fine time scale, but want to acknowledge that there is advection by the coastal current.

6.5. Summary and Conclusions

This study suggests that eddy overturning across the shelf edge front, driven by surface heat flux, is the dominant process that supplies warm and saline Atlantic Water to the continental shelf west of Spitsbergen throughout the winter. Wind induced Ekman transport cannot override the effect of eddies acting to flatten the isopycnals. The heat that the Atlantic Water provides melts the drifting sea ice in the coastal current. Sea ice concentrations therefore decrease northward. Our model suggests that ice formation contributes to the salinity increase in the shelf water during the winter by only a few percent. It appears that the density of Atlantic Water sets the upper salinity limit of the shelf water, a limit that is close to the upper limit of the classic definition of Arctic Water. If saltier water is produced it likely disappears from the shelf as denser water sliding down off the continental slope. Typical cold halocline layers were observed a few times in the modeled region, apparently after periods of southerly winds, rapid melting, and reduced overturning. This water type disappeared soon after formation. The interaction with residual overturning should be investigated further to see whether melting induced formation of a cold halocline layer might be significant along the path where Atlantic Water meets the Arctic sea ice cover. The effect of residual overturning should be taken into consideration when modeling fronts associated with geostrophic currents, in general. The West Spitsbergen Current is a small part of a current system which is sometimes referred to as the Arctic Circumpolar Boundary Current following the continental shelf slope around the Nordic Seas and Arctic Ocean [*Rudels et al*., 1999]. Eddy overturning is likely important along the whole path of that current system, similar to the shelf in the Southern Ocean. In the present work, we have utilized only part of the data collected by the harbor seals west of Spitsbergen during the two winter seasons. The entire seal data set can probably reveal more about the shelf processes west of Spitsbergen.

Appendix A: Seal Data Specifications

Figure A1 shows the positions of all profiling dives made by the adult and subadult harbor seals equipped with CTD-SDRLs. Calibration of the temperature and salinity data was based on intercalibration between tags on seals doing dives within the latitudinal boundaries of the shelf water body domain (78.25°N and 78.7°N, see Figure 1). This included 3160 dives during the 2009–2010 season and 3090 dives during the 2010–2011 season. Calibration was done visually in a temperature-salinity diagram, systematically in the same sequence both seasons. The first step was to calibrate the tag from the seal having most frequent deep dives during March and April, focusing on profiles being warm and saline in the deep, and near freezing point temperature in the surface. For these profiles, the upper salinity bound was set to 35.1 for the deep data, and a lower surface temperature was the freezing point. Supercooling was allowed for in shallow

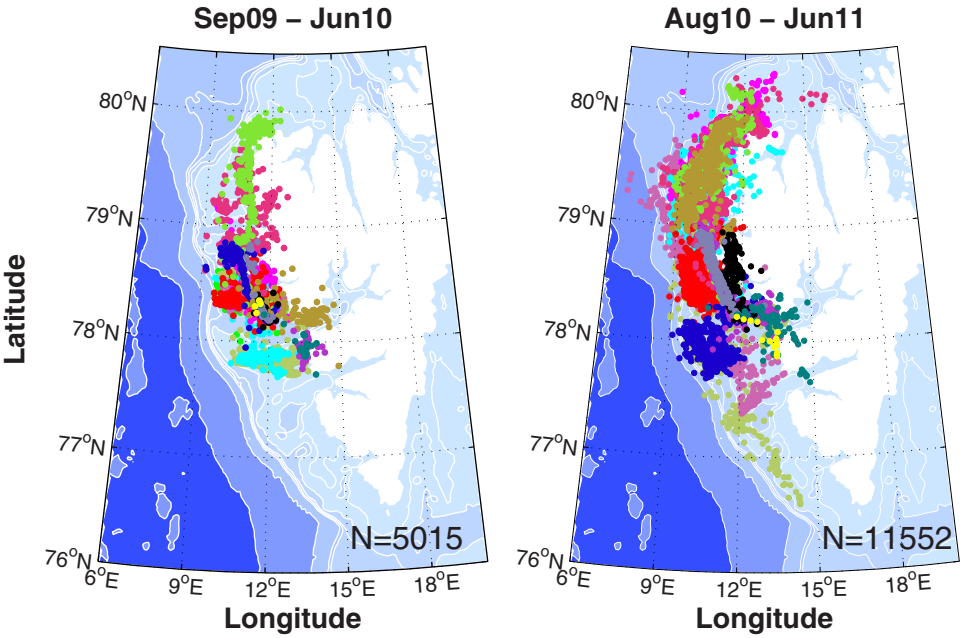

Figure A1. Positions of profiling dives made by (left) 15 harbor seals during the period 1 September 2009 to 17 June 2010 and (right) 14 harbor seals during the period 24 August 2010 to 23 June 2011. Different colors refer to individual seals.

profiles close to the shore. This "base seal" was number 11 during 2009–2010 (that did a total of 692 dives in the domain, 197 of them during March and April), and number 10 during 2010–2011 (that did a total number of 811 dives in the domain, 216 of them during March and April). Intercalibration was performed as follows. Other seals doing dives during the period January through April were visually adjusted to the base seals' tags profiles. (These were seals numbers (1, 3, 4, 6, 7, 8, 9, 10, 12, and 13) in 2010 and (4, 6, 7, 12, and 14) in 2011.) A visual comparison was then done between profiles from May to June, and finally between autumn profiles. The adjustments decided on were all constant in time except for seal 12 in 2010–2011. The conductivity sensor on this particular seal started to drift 12 December 2010 and then stabilized at a higher level 14 January 2011. We are quite certain of this because seals 12 and 10 appeared to dive together during this period. In practice, seals 2, 5, and 15 did not contribute to the data set during 2009–2010, and 3, 5, 9, and 13 did not in 2010–2011. This was because they left the area early in the autumn. The adjustments for winter 2009–2010, for each seal listed from 1 to 15, are for temperature $\delta T = (0; 0; 0; -0.1; 0; 0; 0; -0.05; -0.1; -0.03; 0; -0.07; 0; 0; 0)$°C and for salinity $\delta S = (-0.2; -0.1; -0.1; -0.15; -0.1; -0.2; 0.1; -0.1; -0.1; -0.05; -0.15; -0.15; -0.3; 0.0; 0.2)$ psu. For the second winter 2010–2011, the adjustments are for each seal listed from 1 to 14, temperature $\delta T = (0; 0.015; 0.03; 0; 0.03; 0.02; -0.05; 0; 0; 0.07; -0.05; 0; 0; 0.0)$°C, and salinity $\delta S = (-0.1; -0.1; -0.1; -0.15; -0.1; -0.15; -0.2; -0.1; -0.1; -0.25; -0.1; -0.2; 0.; -0.2)$ psu. Seal 12 initially had no salinity adjustment, but gradually changed to -2 psu from 12 December 2010 to 14 January 2011. In 2009–2010, our references to seals 1–15 correspond to seal tag numbers (94,891–94,905). In 2010–2011, our references to seals number 1–14 correspond to seal tag numbers (53,704–53,719), when excluding number 53,709 because that seal made only one dive.

When selecting the time series data, most profiles outside the domain were excluded from the data set. However, dives up to depths of 300 m were accepted when they were within the latitudinal boundaries, but did not contain purely Atlantic Water. Deep profiles with very typical Atlantic Water were excluded; 10 profiles in 2009–2010 and 20 profiles in 2010–2011. A few dives that took place in the sound between Prins Karls Forland and Spitsbergen were also excluded. These profiles were shaped very differently than the shelf profiles, and included about 10 profiles in 2009–2010 and 20 profiles in 2010–2011. The latitude and longitude of the original dive positions are shown in Figure A2, sorted into day bins. Intercalibrated temperature and salinity values from this time series are shown in Figure A3.

The averaging method used for constructing the single profile time series is described in *Nøst et al.* [2011]. Our pressure bins (5–10, 10–15, 15–20, 20–30, 30–40, 40–50, 50–60, 60–80, 80–100, 100–150, and

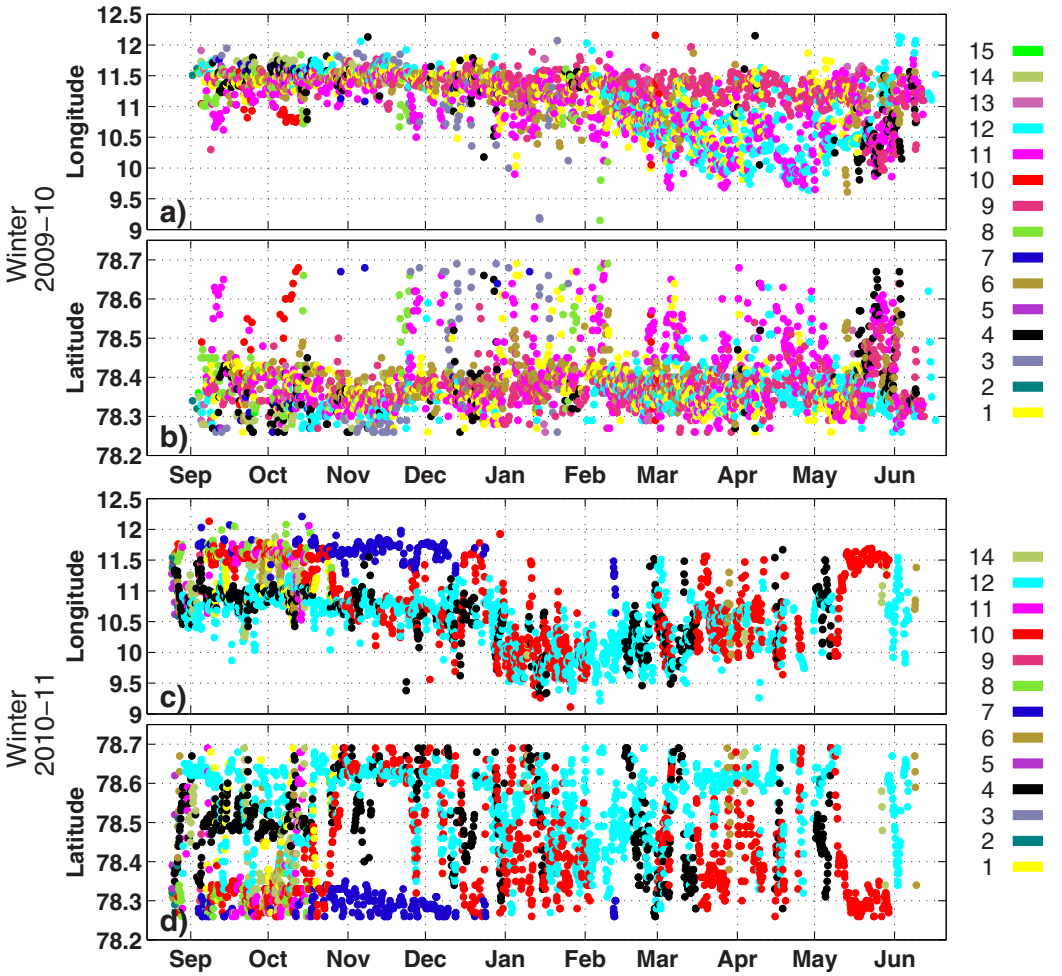

Figure A2. (a and c) Longitude and (b and d) latitude distributions for CTD profiles inside the geographical domain shown in Figure 1. Colors refer to individual seals.

150–200 dbar) and time bins (14 day periods) do however deviate from that description. The number of samples and standard deviations of salinity and temperature in each bin is shown in Figure A4. TS plots of original observations are shown in Figure A5 from selected days. Original observations from their corresponding 14 day time bins are shown in Figure 4.

Appendix B: Heat and Freshwater Budget Model Specifics

The shelf width-weighted and depth-integrated heat content

$$q_{vol}(t) = \int_{z=-H}^{0} c_{pw}\,\rho_w\,(T(z,t) - T_f)\,W(z)dz \tag{B1}$$

and freshwater content

$$F_{vol}(t) = \int_{z=-H}^{0} \rho_w\,(S_{ref} - S(z,t))\,W(z)dz. \tag{B2}$$

used in equation (2) were calculated from the smoothed profile time series of temperature $T(z, t)$ and salinity $S(z, t)$ shown in Figure 5, weighted with the north-south averaged shelf width profile $W(z)$ of the domain, integrated from the deepest bottom depth (H = 200 m; western boundary) to the surface. The shelf width

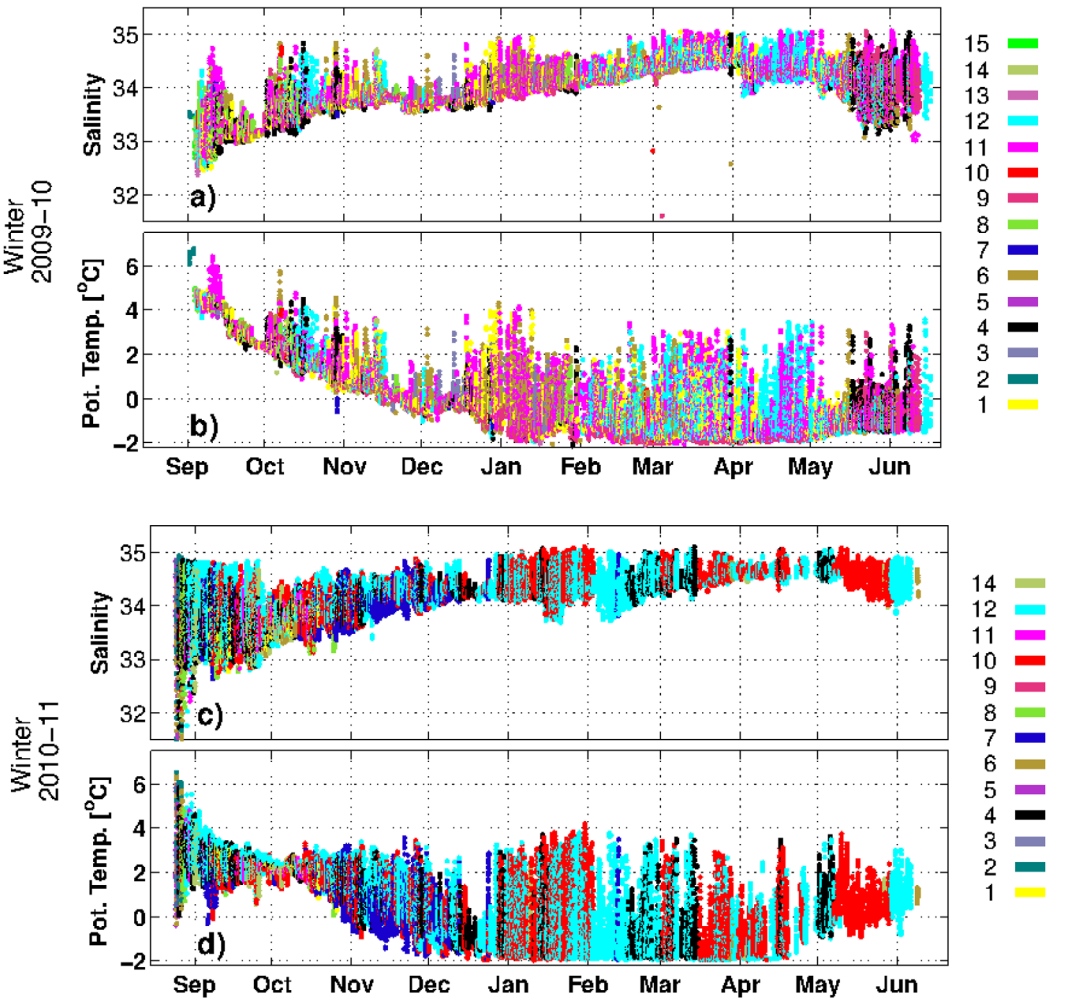

Figure A3. Time series of all intercalibrated (a and c) salinity and (b and d) temperature data within the geographical domain in Figure 1. Colors refer to individual seals.

profile calculated from the IBCAO bathymetric map is approximately (27, 26, 26, 25.5, 25.5, 25, 24, 23, 22, 20, 11, and 2) km at the corresponding depths (0, 10, 15, 20, 30, 40, 50, 60, 80, 100, 150, and 200) m, respectively. A reference salinity $S_{ref} = 35.1$ is set to the typical salinity of Atlantic Water in the core of the West Spitsbergen Current and T_f is seawater freezing temperature. Specific heat of seawater c_{pw} (J kg^{-1}°C^{-1}) and density of seawater ρ_w (kg m^{-3}) has appropriate values associated with $T(z, t)$ and $S(z, t)$. Note that to get the actual heat and freshwater contents in the geographical domain, q_{vol} (J m^{-1}) and F_{vol} (kg m^{-1}) have to be multiplied by the north-south extension of the domain (50 km). The time lapse Δt was set to 1 day. Shelf width-weighted and depth-averaged temperature $\bar{T}(t)$ and salinity $\bar{S}(t)$ in equation (4) are calculated as:

$$\bar{T}(t) = \frac{\int_{z=-H}^{0} T(z,t)W(z)dz}{\int_{z=-H}^{0} W(z)dz} \wedge \bar{S}(t) = \frac{\int_{z=-H}^{0} S(z,t)W(z)dz}{\int_{z=-H}^{0} W(z)dz}. \quad \text{(B3)}$$

Heat and freshwater contents of surface and bottom shelf water parcels (q_s, F_s, q_b, and F_b in equations (6) and (7)) are calculated from seal data temperatures and salinities from the shallowest (0–10 m) and deepest (150–200 m) depth bins, in a manner similar to equation (4), with $\bar{T}$ and $\bar{S}$ values being replaced by surface and bottom values. Similarly, Atlantic Water heat specification (q_{aw} in equation (6)) is calculated by a formula similar to equation (4) with T_{aw} replacing $\bar{T}$ and specific heat capacity and density corresponding to

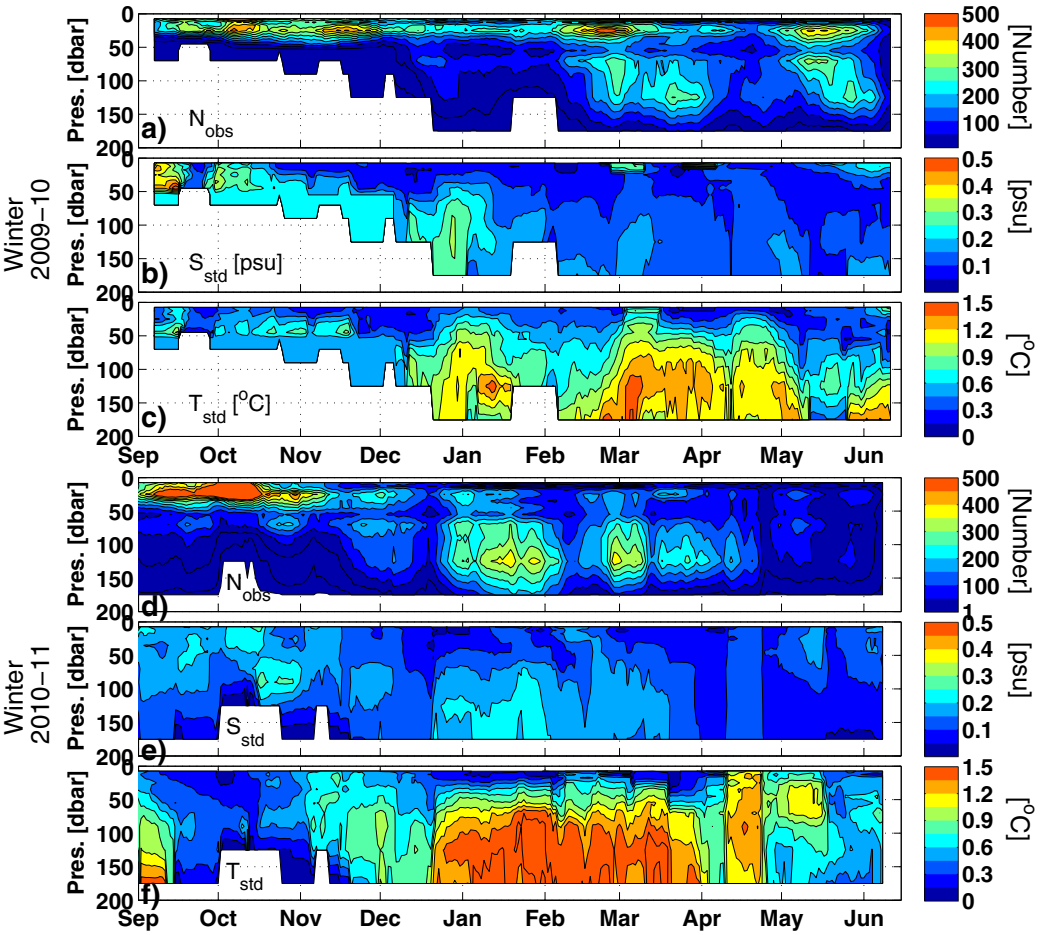

Figure A4. Hovmöller diagrams of (a and d) numbers of observations, (b and e) standard deviation of salinity (in psu), and (c and f) standard deviation of temperature (in °C) within each time-pressure data bin inside the geographical domain shown in Figure 1.

Atlantic Water values. T_{aw} decreases linearly from 5°C in mid-September to 3.5 ± 0.5°C in mid-March. Since Atlantic Water has the reference salinity S_{ref} it contains no freshwater by definition.

Sea ice cover data used for parameter a in equation (5) was downloaded from the NSIDC (National Snow & Ice Data Center) gridded daily data set, using the average values within the geographical region (78.3°N–78.6°N, 10°E–11°E). Net precipitation minus evaporation in the freshwater budget (equation (2)) is expressed

$$F_{pe}(t) = [1 - a(t)]\,[P(t) - E(t)]\rho_w W(0), \tag{B4}$$

where P is precipitation and E is evaporation, with units in meters during 1 day. P and E are downloaded ERA-Interim data from a position in the middle of the modeled shelf region.

Heat flux Q_a (J s^{-1} m^{-2}) through the ocean surface is the sum of net shortwave (solar) radiation Q_{sw}, net longwave radiation Q_{lw}, turbulent sensible heat flux Q_{sh}, and turbulent latent heat flux Q_{lh}. All four of these surface heat flux terms are expressed with empirical bulk formulae, basically following *Renfrew et al.* [2002]. Input data needed for each heat flux term indicated inside the brackets:

$$Q_a = Q_{sw}(r_w, N) + Q_{lw}(T_{sst}, N) + Q_{sh}(U_{10}, T_{air}, T_{sst}) + Q_{lh}(U_{10}, r_w, T_{air}), \tag{B5}$$

are relative humidity (r_w), cloud cover (N), sea surface temperature (T_{sst}), wind 10 m above the ground (U_{10}), and air temperature 2 m above the ground (T_{air}). We extracted U_{10} from the atmospheric reanalysis ERA-Interim data set [*Dee et al.*, 2011] provided by ECMWF (European Centre for Medium-Range Weather Forecasts) from a position centered in the model domain (78.5°N, 10.5°E), while r_w, N, and T_{air} were observations from a weather station in Ny Ålesund (position: 78.92°N, 11.92°E, 50 km east of the domain) serviced by the Norwegian Polar

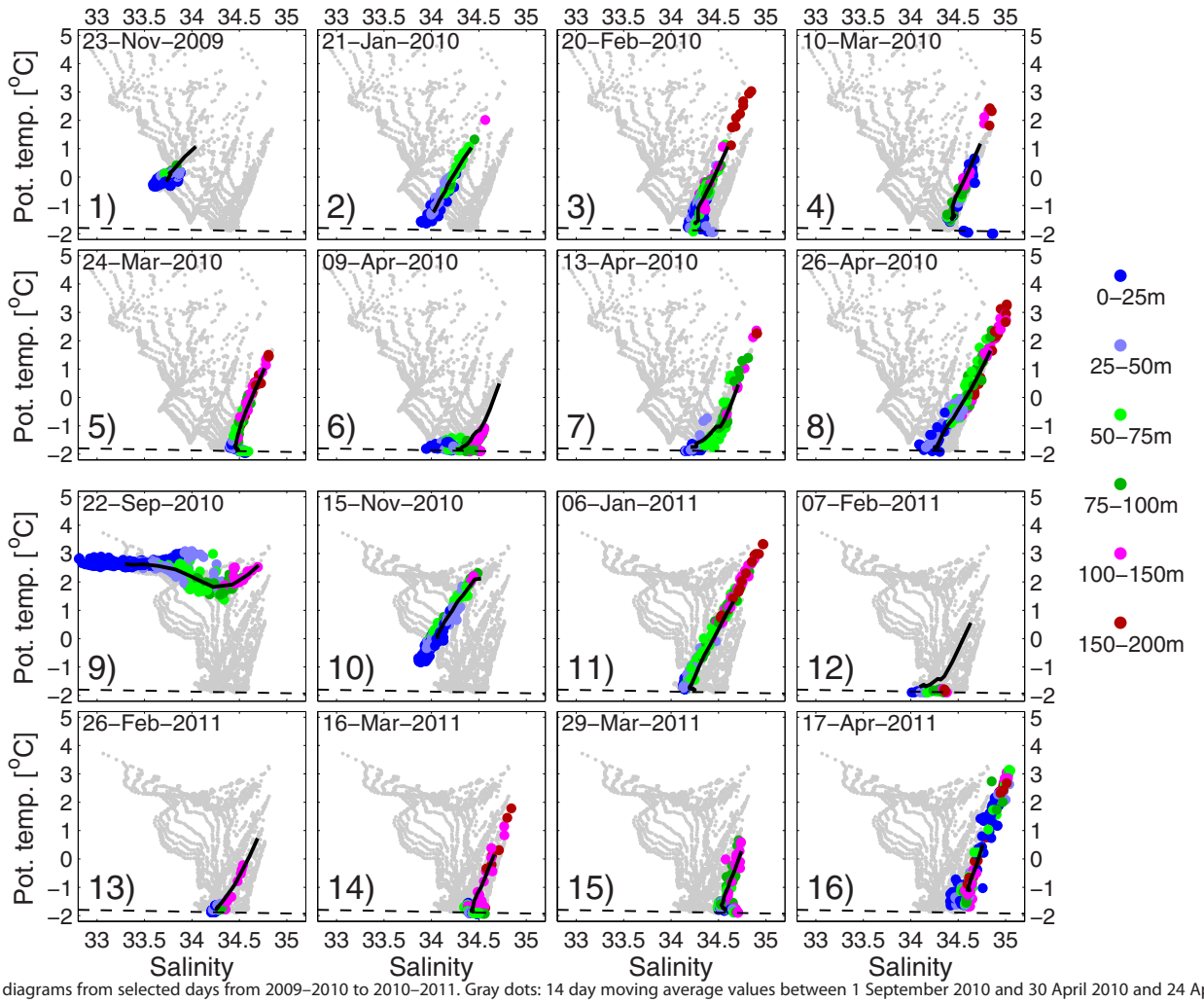

Figure A5. TS diagrams from selected days from 2009–2010 to 2010–2011. Gray dots: 14 day moving average values between 1 September 2010 and 30 April 2010 and 24 April 2011. Black solid line: average profile from the selected day.

Institute. During a 2 week period of no observations (19 December 2009 to 4 January 2010), the Ny Ålesund data were replaced by data from Longyearbyen (position: 78.23°N, 15.36°E, 100 km further south-east.) serviced by the Norwegian Weather Service (met.no) see section 6.4 for a discussion around this approach. All data sets giving inputs to equation (B5) have a time resolution of 6 h, however for model use they are averaged into daily means. Sea surface temperature T_{sst} is extracted from daily means from the seal borne instruments at 6 m.

Our approach deviates from *Renfrew et al.* [2002] in that we use a constant albedo ($\alpha = 0.08$), and we use different coefficients in the formula for clear sky downwelling radiation SWD_{CLEAR}:

$$SWD_{CLEAR} = \frac{S_0 \cos^2 Z}{1.2\cos Z + (2.7 + \cos Z)e_a + 0.06}, \tag{B6}$$

where Z is the solar zenith angle, e_a is the vapor pressure in bars (recalculated from relative humidity r_w through $e_a = r_w e_w(T_{air})$, where $e_w(T_{air})$ is the saturation vapor pressure in bars at air temperature T_{air}), and the solar constant $S_0 = 1370$ W m^{-2}. Equation (B6) is analogous to the method used by *Curry and Webster* [1999] (following *Renfrew et al.* [2002]) except for the first and last constant coefficients in the denominator. Our expression leads to close agreement with output from the SBDART software [*Ricchiazzi et al.*, 1998] under the conditions of clear sky and no aerosols, between wavelengths 0.2 and 3 μm. We have calculated the solar zenith angle Z by using an algorithm suggested by *Reda and Andreas* [2003], with daily values estimated as daily averages of hourly values, using 90° as a maximum value (i.e., angles above 90° are replaced by 90°). We refer to *Renfrew et al.* [2002] for further description of terms in equation (B5)

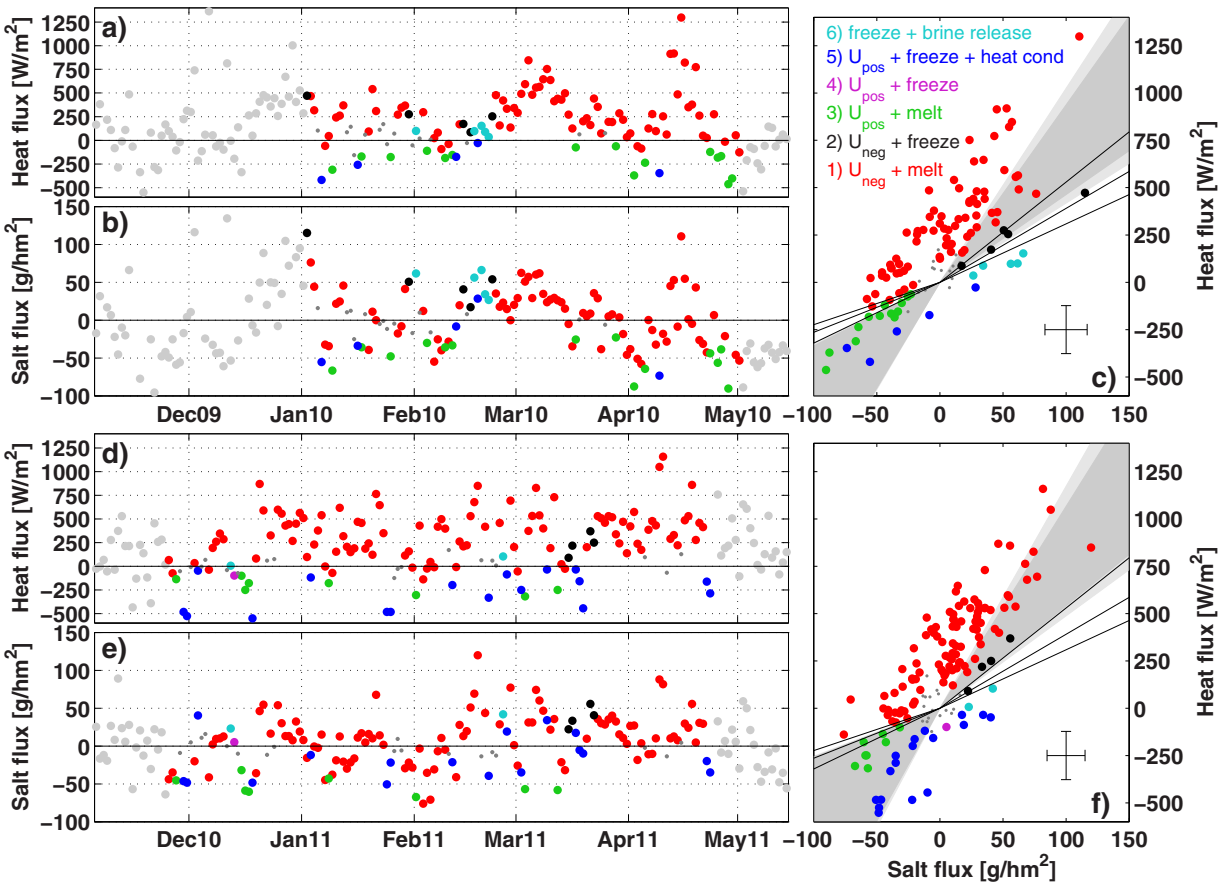

Figure A6. (a and d) Observed heat change scaled to heat flux equivalents (W m^{-2}), after subtracting specified heat exchange with the atmosphere and northward advection of shelf water. (b and e) Observed salt change scaled to salt flux equivalents (g salt per hour and surface m^2), after subtracting specified precipitation, evaporation, and northward advection of shelf water. (c and f) The data from Figures A6a, A6b, A6d, and A6e plotted in flux space. Color code refer to the model selected paired processes (1–4 with exceptions 5 and 6). Black lines: three freezing lines from equation (C5) (positive salt flux, and $S_{diff} = 14$, 19, and 24 psu) and three melting lines from equation (C2) (negative salt flux, and $S_i = 2$, 7, and 12 psu). Shaded gray areas: negative overturning cell from equation (C2) (positive heat and salt fluxes and $T_{aw} \pm 0.5^{\circ}$C) and positive overturning cell from equation (C3) (negative heat and salt fluxes). In lower right corners: ±mean standard errors (equation (C6)).

We define Arctic Water [*Loeng*, 1991] as having a constant salinity close to the end product of the winter season, $S_{arw} = 34.6$, with a temperature T_{arw} that decreases linearly from 1°C in September to freezing temperature in mid-March. Its heat specification q_{arw} and freshwater content F_{arw} (in equation (12)) is defined by a formula similar to equation (4) with T_{arw} and S_{arw} replacing $\bar{T}$ and $\bar{S}$, and specific heat and density corresponding to Arctic Water values. Arctic Water volume flux is estimated from the formula $U_{arw} = v_{arw}\bar{W}\bar{H}/L_{arw}$, where v_{arw} is advection speed, $\bar{W}$ is the mean width, $\bar{H}$ the mean depth of the model domain, and L_{arw} is the distance to the source water. In the model, it is assumed that the source water is located 100 km south of the domain (at Sørkapp), and that the advection speed is 1 cm s^{-1}, implying $U_{arw} \approx 0.3$ m^2 s^{-1}.

Appendix C: Budget Model Solution Method

The prescribed terms (q_{adv}, F_{adv}, and q_{surf}) are subtracted from equation (2), defining two new delta parameters:

$$\begin{aligned}\delta q_{vol}(t) &= q_{vol}(t+\Delta t) - q_{vol}(t) - q_{surf}(t) - q_{adv}(t) = q_{res}(t) + q_m(t) + q_{fr}(t)\\ \delta F_{vol}(t) &= F_{vol}(t+\Delta t) - F_{vol}(t) - F_{adv}(t) - F_{pe}(t) = F_{res}(t) + F_m(t) + F_{fr}(t),\end{aligned} \tag{C1}$$

which are known since q_{vol} and F_{vol} are determined from the seal data time series shown in Figures 5 and 9. The delta parameters δq_{vol} and δF_{vol} define a vector in a heat and freshwater flux-space. Each of the processes on the right-hand side of equation (C1) will, when determined, form vectors in the same space, and

the slopes of the different vectors are easily determined from the process definitions. From equation (6), it can be seen that a negative overturning cell would cause changes in heat and salt in the model domain along the following slope:

$$\frac{q_{neg}}{F_{neg}} = \frac{q_s - q_{aw}}{F_s}, \tag{C2}$$

with decreasing freshwater content. Positive overturning would cause changes along the slope following equation (7) as

$$\frac{q_{pos}}{F_{pos}} = \frac{q_s - q_b}{F_s - F_b}, \tag{C3}$$

with freshwater content increasing. Sea ice melting would (see equation (10)) cause changes along the melting line

$$\frac{q_m}{F_m} = \frac{L_i}{S_i - S_{ref}}, \tag{C4}$$

and results in the addition of freshwater. Sea ice formation from equation (11) would cause changes along the freezing line

$$\frac{q_{fr}}{F_{fr}} = \frac{L_i}{S_{ifr} - S_s} = \frac{L_i}{-S_{diff}}, \tag{C5}$$

resulting in increases in the salt content.

Equation (C1) has dimensions (J m^{-1}) and (kg m^{-1}), and is associated with changes in total heat and freshwater in the domain during one model time step (1 day in the present set up). These are converted into (W m^{-2}) (equivalent to surface heat flux) and to (g m^{-2} h^{-1}) (equivalent with salt flux from the ice during sea ice formation), with the h being per hour [*Notz and Worster*, 2008]. This conversion requires that numerators in equations (C1)–(C5) are divided by $(W(0)\Delta t)$ and the denominators by $(-24W(0))$. The minus sign shifts freshwater flux to salt flux.

The converted flux delta parameters from equation (C1) are plotted in Figure A6, both with time (left plots) and in heat and salt flux-space (right plots). The observed fluxes (dots in Figure A6) can be expressed as a sum of vectors representing the four processes involved, where the length of each vector is determined by the tuning parameters in the model: U_{neg}, U_{pos}, d_m, and d_{fr}.

The solution method tests the following four combinations: (1) negative overturning (Atlantic Water entering the domain at depth) and melting ice (U_{neg} and d_m); (2) negative overturning and ice freezing at the surface (U_{neg} and d_{fr}); (3) positive overturning and ice melting (U_{pos} and d_m); or (4) positive overturning and ice freezing (U_{pos} and d_{fr}), and selects the pair of process vectors that can create the observed delta parameter flux vector. Two exceptions are found. The first is a situation when cooling of the domain is larger than any combination of processes can explain (defined as situation 5, with blue dots in Figure A6). Under this scenario excess cooling q_u is introduced and linked to a larger heat loss to the atmosphere than the surface heat flux data suggest (see Figure 6 where also adjustments from q_u to the surface heat flux are indicated). Alternatively, it can be explained by heat conduction into the drift ice. The second exception occurs when some extra salt release d_{frI} is needed (defined as situation 6, with cyan dots in Figure A6). Such a situation can interpreted as a result of salt release from newly formed sea ice.

Error estimates are based on classic theory [*Taylor*, 1982], where uncertainty of salinity and temperature in each pressure-time bin is

$$\delta_{n,k} = \frac{\sigma_{n,k}}{\sqrt{N_{n,k}}}, \tag{C6}$$

where σ is standard deviation and N is number of observations in each pressure (index k) and time (index n) bin. The error influence on the different terms in the model (equation (2)) is based on fractional uncertainties [see *Nøst et al.*, 2011].

Sensitivity testing, shown in Figure 7, is based on the 0.5°C uncertainty in T_{aw} as well as 5 psu uncertainty in drift ice salinity ($S_i = 7 \pm 5$ psu) as well as brine release during ice formation. Newly formed sea ice is

assumed to add a constant amount of salinity $S_{diff} = S_s - S_{ifr} = 19 \pm 5$ psu to the water column for each unit of sea ice formed in each time step. An approach that assumes a constant S_{diff} was chosen because it results in a parameter for ice freezing that is easy to compare with the ice melting parameter. Sea ice formation during turbulent conditions has been shown to induce a salt flux of 40 g m^{-2} h^{-1} into the water column in Adventfjorden, Svalbard [*Notz and Worster*, 2008]. This salt flux value corresponds to formation of sea ice that is 5.5 cm during 1 day when the salt difference is 19 psu.

Acknowledgments
The seal-based CTD data collection was financed by a Norwegian Research Council project 184644/s40 (KMK), with additional funding provided by the Norwegian Polar Institute. For data access, contact kit.kovacs@npolar.no. We would like to thank Helen Flå, Knut Flå, Kathy Frost, Lisa Leclerc, Lloyd Lowry, Benjamin Merkel, Morten Tryland, and Bjorn Waalberg for their assistance in the capture and tagging of the harbor seals instrumented in this study.

References

Alexev, V. A., V. V. Ivanov, R. Kwok, and L. H. Smedsrud (2013), North Atlantic warming and declining volume of arctic sea ice, *Cryosphere Discuss.*, *7*, 245–265.

Boyd, T., and E. D'Asaro (1994), Cooling of the West Spitsbergen Current: Wintertime observations west of Svalbard, *J. Geophys. Res.*, *99*, 22,597–22,618.

Cottier, F., F. Nilsen, M. E. Inall, S. Gerland, V. Tverberg, and H. Svendsen (2007), Wintertime warming of an Arctic shelf in response to large-scale atmospheric circulation, *Geophys. Res. Lett.*, *34*, L10607, doi:10.1029/2007GL029948.

Curry, J. A., and P. J. Webster (1999), *Thermodynamics of Atmospheres and Oceans*, 471 pp., Academic, San Diego, Calif.

Dee, D. P., et al. (2011), The ERA-Interim reanalysis: Configuration and performance of the data assimilation system, *Q. J. R. Meteorol. Soc.*, *137*, 553–597.

Hegseth, E. N., and V. Tverberg (2013), Effect of Atlantic water inflow on the timing of the phytoplankton spring bloom in a high Arctic fjord (Kongsfjorden, Svalbard), *J. Mar. Syst.*, *113–114*, 94–105.

Ivanov, V., V. A. Alexev, I. Repina, N. V. Koldunov, and A. Smirnov (2012), Tracing Atlantic Water signature in the arctic sea ice cover east of Svalbard, *Adv. Meteorol.*, Article ID 201818, 11 pp., doi:10.1155/2012/201818.

Loeng, H. (1991), Features of the physical oceanographic conditions of the Barents Sea, *Polar Res.*, *10*, 5–18.

Marshall, J., and T. Radko (2003), Residual-mean solutions for the Antarctic Circumpolar Current and its associated overturning circulation, *J. Phys. Oceanogr.*, *33*, 2341–2354.

Marshall, J., H. Jones, R. Karsten, and R. Wardle (2002), Can eddies set ocean stratification?, *J. Phys. Oceanogr.*, *32*, 26–38.

Marshall, J., E. Shuckburgh, H. Jones, and C. Hill (2006), Estimates and implications of surface eddy diffusivity in the Southern Ocean derived from tracer transport, *J. Phys. Oceanogr.*, *36*, 1806–1821.

Nilsen, F., B. Gjevik, and U. Schauer (2006), Cooling of the West Spitsbergen Current: Isopycnal diffusion by topographical vorticity waves, *J. Geophys. Res.*, *111*, C08012, doi:10.1029/2005JC002991.

Nøst, O. A., M. Biuw, V. Tverberg, C. Lydersen, T. Hattermann, Q. Zhou, L. H. Smedsrud, and K. M. Kovacs (2011), Eddy overturning of the Antarctic Slope Front controls glacial melting in the Eastern Weddell Sea, *J. Geophys. Res.*, *116*, C11014, doi:10.1029/2011JC006965.

Notz, D., and M. G. Worster (2008), In situ measurements of the evolution of young sea ice, *J. Geophys. Res.*, *113*, C03001, doi:10.1029/2007JC004333.

Reda, I., and A. Andreas (2003), Solar position algorithm for solar radiation application, *Tech. Rep. NREL/TP-560–34302*, Natl. Renewable Energy Lab., Golden, Colo., doi:10.2172/15003974.

Renfrew, I. A., J. C. King, and T. Markus (2002), Coastal polynyas in the southern Weddell Sea: Variability of the surface energy budget, *J. Geophys. Res.*, *107*(C6), doi:10.1029/2000JC000720.

Ricchiazzi, P., S. Yang, C. Gautier, and D. Sowle (1998), SBDART: A research and teaching software for plane-parallel radiative transfer in the earth's atmosphere, *Bull. Am. Meteorol. Soc.*, *79*, 2101–2114.

Rudels, B., L. G. Anderson, and E. P. Jones (1996), Formation and evolution of the surface mixed layer and halocline of the Arctic Ocean, *J. Geophys. Res.*, *101*, 8807–8821.

Rudels, B., H. J. Friedrich, and D. Quadfasel (1999), The Arctic Circumpolar Boundary Current, *Deep Sea Res., Part II*, *46*(6–7), 1023–1062.

Sirevaag, A. (2009), Turbulent exchange coefficients for the ice/ocean interface in case of rapid melting, *Geophys. Res. Lett.*, *36*, L04606, doi:10.1029/2008GL036587.

Sirevaag, A., and I. Fer (2009), Early spring oceanic heat fluxes and mixing observed from drift stations north of Svalbard, *J. Phys. Oceanogr.*, *39*, 3049–3069.

Steele, M., J. Morison, and T. B. Curtin (1995), Halocline water formation in the Barents Sea, *J. Geophys. Res.*, *100*, 881–894.

Stewart, A. L., and A. F. Thompson (2013), Connecting Antarctic cross-slope exchange with Southern Ocean overturning, *J. Phys. Oceanogr.*, *43*, 1453–1471.

Taylor, J. R. (1982), *An Introduction to Error Analysis: The Study of Uncertainties in Physical Measurements*, 329 pp., Univ. Sci. Books, Mill Valley, Calif.

Tverberg, V., and O. A. Nøst (2009), Eddy overturning across a shelf edge front: Kongsfjorden, west Spitsbergen, *J. Geophys. Res.*, *114*, C04024, doi:10.1029/2008JC005106.